Synthesis and Physical Investigation of Donor–Donor and Acceptor–Acceptor End-Functionalized Monodisperse Poly(triacetylene) Oligomers

Rainer E. Martin,[a, d] Ulrich Gubler,[b] Corinne Boudon,[c] Christian Bosshard,[b] Jean-Paul Gisselbrecht,[c] Peter Günter,[b] Maurice Gross,[c] and François Diederich*[a]

Abstract: Two series of monodisperse, terminally donor–donor [D–D, D = 4-(dimethylamino)phenyl] and acceptor–acceptor [A–A, A = 4-nitrophenyl] functionalized poly(triacetylene) (PTA) oligomers ranging from monomer to hexamer were synthesized by oxidative Hay oligomerization under end-capping conditions. The corresponding D–D and A–A end-substituted polymers with an average degree of polymerization (DP) of $n \approx 18$ and $n \approx 12$, respectively, were also prepared and served as reference points for the corresponding infinitely long polymers. These terminally functionalized PTA oligomers and polymers are yellow- to orange-colored compounds, displaying excellent solubility in aprotic solvents with melting points above 200 °C for the hexamers. For the 4-(dimethylamino)phenyl substituted compounds, a consistent first oxidation potential around +0.42 V versus Fc/Fc$^+$ (ferrocene/ferricinium) was observed, whereas the 4-nitrophenyl functionalized systems underwent a reversible reductive two-electron transfer around −1.40 V versus Fc/Fc$^+$. The nature of the end-groups has a dramatic influence on the electronic absorption spectra. Saturation of the linear optical properties in the D–D series occurs at significantly shorter chain-length [effective conjugation length (ECL) of $n \approx 4$ monomer units] than in the A–A substituted or the previously reported Me_3Si- and Et_3Si-end-capped PTA oligomer series (ECL: $n \approx 10$ monomer units). Similar observations with respect to the ECL were made by measurement of the Raman-active $\tilde{\nu}_{(C\equiv C)}$ stretches. Third-harmonic generation (THG) and degenerate four-wave mixing (DFWM) experiments showed that shorter oligomers of terminally D–D or A–A functionalized PTAs display higher second hyperpolarizabilities γ than the corresponding R_3Si-end-capped series (R = alkyl). Moreover, they disclose a distinct peak of the nonlinearity per monomer unit at intermediate backbone lengths. In THG experiments, the second hyperpolarizabilities for long D/A-functionalized PTA oligomers attained the same saturation values as observed for the corresponding R_3Si-end-capped rods. The nonlinearities measured by DFWM of the D–D and A–A substituted PTAs were found to be larger than for the silylated ones, which can be explained by the closeness of the two-photon resonance.

Keywords: alkynes · molecular wires · effective conjugation length · Raman spectroscopy · nonlinear optics

Introduction

Monodisperse, soluble oligomers with precisely defined length and constitution continue to raise large interest as model compounds for linearly π-conjugated polymers.[1–6] We reported in the past the synthesis and study of two series of monodisperse trialkylsilyl-end-capped poly(triacetylene) (PTA) oligomers. The first series, with terminal Me_3Si groups, extended from the 0.96 nm long monomer **1a** to the 4.61 nm long hexameric oligomer **1f** and displayed high solubility in common organic solvents, allowing a first investigation of structure–property relationships in PTAs.[7] By extrapolative evaluation of linear and third-order nonlinear optical properties, utilizing the two polydisperse polymer samples **2a** and **2b** that already displayed saturation in their linear and nonlinear optical properties and therefore served as data points for an

[a] Prof. Dr. F. Diederich, Dr. R. E. Martin
Laboratorium für Organische Chemie, ETH-Zentrum
Universitätstrasse 16, 8092 Zürich (Switzerland)
Fax: (+41) 1-632-1109
E-mail: diederich@org.chem.ethz.ch

[b] Dr. U. Gubler, PD Dr. C. Bosshard, Prof. Dr. P. Günter
Nonlinear Optics Laboratory
Institute of Quantum Electronics, ETH-Hönggerberg
8093 Zürich (Switzerland)

[c] Dr. C. Boudon, Dr. J.-P. Gisselbrecht, Prof. Dr. M. Gross
Laboratoire d'Electrochimie et de Chimie Physique du Corps Solide
Université Louis Pasteur—C.N.R.S.: U.M.R. No. 7512
Faculté de Chimie
4 rue Blaise Pascal, 67000 Strasbourg (France)

[d] Dr. R. E. Martin
current address:
F. Hoffmann-La Roche Ltd, Pharmaceuticals Division
4070 Basel, Switzerland

0947-6539/00/0623-4400 $ 17.50+.50/0

infinitely long polymer, the effective conjugation length (ECL) in PTAs was estimated to comprise 7 to 10 monomer units or 42 to 60 C atoms.[7] The ECL defines the number of repeat or monomer units needed in a given linearly π-conjugated polymer to furnish size-independent optical, redox, or other physical properties.[8, 9] To obtain a more direct experimental determination of the ECL,[10–14] we prepared the monodisperse PTA oligomer series **3a–g**

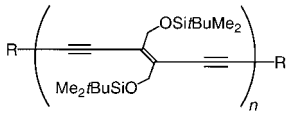

1a-f R = $SiMe_3$ n = 1-6

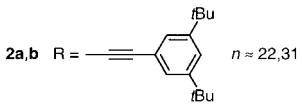

2a,b R = $n \approx 22,31$

3a-g R = $SiEt_3$ n = 1,2,4,6,8,12,16

extending up to a 11.9 nm long hexadecameric (**3g**) PTA rod.[15, 16] This dramatically expanded series with Et_3Si end-groups bridged the gap between the oligomer and polymer domains and allowed a detailed investigation of the physical properties in PTAs up to the interesting regime where physical properties start to show behavior of saturation.

In order to study the influence of electron-releasing [4-(dimethylamino)phenyl] and -withdrawing (4-nitrophenyl) substituents on the physical properties of PTAs, we have now prepared two series of terminally donor–donor (D–D; **4a–f**) and acceptor–acceptor (A–A; **5a–f**) functionalized oligomers ranging from monomer to hexamer by oxidative Hay polymerization under end-capping conditions. The corresponding polydisperse D–D and A–A PTA polymers **4g** and **5g** with average degrees of polymerization (DP) of $n \approx 18$ and $n \approx 12$, respectively, allow further useful structure–property correlations. Here, we report the synthesis, characterization, and comprehensive physical study (electro-

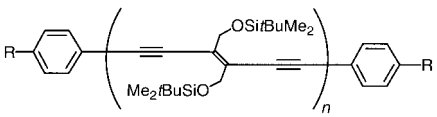

4a-g R = NMe_2 n = 1-6, ≈ 18

5a-g R = NO_2 n = 1-6, ≈ 12

chemistry, linear and nonlinear optical properties, Raman scattering) of these new compounds. The comparison with their previously reported silyl-end-capped counterparts demonstrates that the nature of the end-groups can have a large influence on physical properties and induce dramatic changes in the ECL as revealed by electronic absorption spectroscopy.

Results and Discussion

Synthesis and characterization: The donor or acceptor substituted *trans*-diethynylethenes [DEEs, (*E*)-hex-3-ene-1,5-diynes] **6** and **7** were prepared as end-capping reagents starting from mono-silyl-protected DEE **8**[17, 18] (Scheme 1). Sonogashira-type cross-coupling[19] of **8** with 4-iodo-*N*,*N*-dimethylaniline or 4-iodonitrobenzene afforded **9** and **10**,

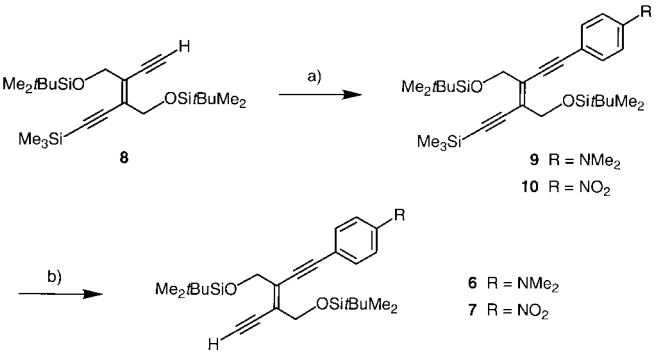

Scheme 1. Synthesis of end-capping units **6** and **7**. a) 4-Iodo-*N*,*N*-dimethylaniline or 4-iodonitrobenzene, $[PdCl_2(PPh_3)_2]$, CuI, NEt_3, 20 °C, 24 h, **9**: 85%, **10**: 95%. b) NaOH, THF/MeOH 1:1, 20 °C, 2 h, **6**: 90%, **7**: 93%.

respectively, and removal of the Me_3Si-protecting group gave the end-capping reagents which could be stored at −20 °C for extended periods of time without decomposition.

The preparation of the two monomers **4a**[17, 18] and **5a**[20] has been previously described. The synthesis of the new oligomers **4b–f** and **5b–f** was accomplished by oxidative Hay polymerization of *trans*-enediyne **11**[21, 22] in the presence of end-capping units **6** and **7**, respectively (Scheme 2).[23] To a first

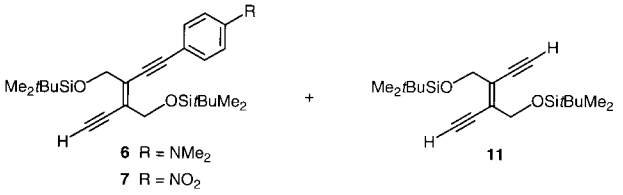

		n	yield [%]
R = NMe_2	**4b**	2	62%
	4c	3	18%
	4d	4	7%
	4e	5	4%
	4f	6	2%
	4g	≈ 18	3%

		n	yield [%]
R = NO_2	**5b**	2	62%
	5c	3	20%
	5d	4	7%
	5e	5	3%
	5f	6	2%
	5g	≈ 12	4%

Scheme 2. Synthesis of D/A-end-capped oligomers **4b–f** and **5b–f** and polymers **4g** and **5g**, respectively. a) CuCl, *N*,*N*,*N*′,*N*′-tetramethylethylenediamine (TMEDA), CH_2Cl_2, 4 Å molecular sieves, air, 20°, 2 h.

approximation, the rate of polymerization was found to be hardly influenced by the terminal D/A functionalities compared with the corresponding Me_3Si- (as in **8**) or Et_3Si-end-capping units, and stirring in a open vessel for 2 h at 20 °C was found to be sufficient for completion of the reaction in both cases. Oligomers **4b–f** and **5b–f** were isolated by preparative

  0947-6539/00/0623-4401 $ 17.50+.50/0

size-exclusion chromatography (SEC, 5×180 cm glass column filled with Bio-Rad Bio-Beads SX-1, CH_2Cl_2) (Figure 1). Final purification of the oligomers was achieved by precipitation of concentrated solutions of the compounds from CH_2Cl_2 with MeOH and subsequent isolation of the solid material by centrifugation.

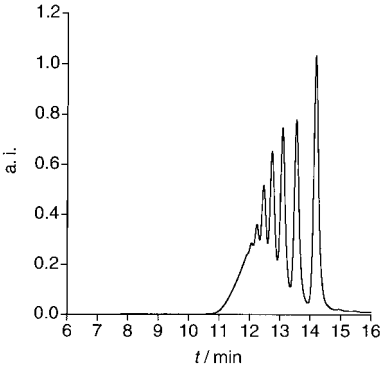

Figure 1. Analytical SEC traces (Bio-Rad Bio-Beads SX-1, CH_2Cl_2) of the crude reaction mixture taken directly after work-up of the oxidative oligomerization of **11** in the presence of end-cap **6**. From right to left (t_R = retention time): dimer **4b** ($t_R = 14.19$ min), trimer **4c** ($t_R = 13.55$ min), tetramer **4d** ($t_R = 13.08$ min), pentamer **4e** ($t_R = 12.74$ min), and hexamer **4f** ($t_R = 12.46$ min), detected at $\lambda = 400$ nm; a.i. = arbitrary units.

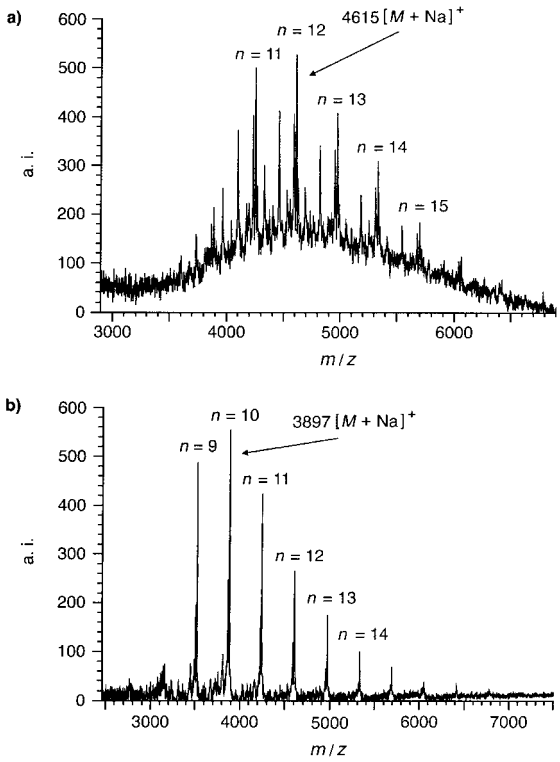

Figure 2. MALDI-TOF mass spectra of a) **4g** [matrix: 2′,4′,6′-trihydroxyacetophenone (THA)/ammonium hydrogencitrate (AHC)] and b) **5g** [matrix: 3-(3-indolyl)acrylic acid (IAA)]. For both polymers, the $[M+Na]^+$ peak was the most intense, followed by $[M]^+$ and $[M - C(CH_3)_3]^+$). In the case of the D–D polymer **4g**, an additional fragmentation peak $[M - OSi(CH_3)_2C(CH_3)_3]^+$ was observed.

Isolated yields of single oligomers were found to be strongly dependent on the ratio of monomer **11** to end-capping reagents **6** and **7**. For instance, using **7** and **11** in a ratio of 4:1 allowed isolation of the A–A oligomers **5b–f** in the yields depicted in Scheme 2, whereas a 2:3 ratio of **7** to **11** resulted in a considerable shift of the product distribution towards higher oligomers (**5b**: 32%, **5c**: 20%, **5d**: 14%, **5e**: 8%, **5f**: 6%). Using a ratio of 2:3 of end-caps **6** or **7** to repeating monomer **11** guaranteed end-capping of both free terminal acetylenes of the π-conjugated chain to a high degree of certainty. This is of crucial importance as subsequent separations of mixtures of incompletely functionalized polymers are not feasible.

Of both D–D and A–A polymerization mixtures, the fastest eluting fractions from the preparative SEC columns were collected and provided samples for end-functionalized polydisperse D–D and A–A PTA polymers (**4g**: $n \approx 18$, $M_w/M_n = 2.04$ and **5g**: $n \approx 12$, $M_w/M_n = 1.65$). They are deep yellow-orange and red solids, respectively, with good solubility in aprotic solvents such as $CHCl_3$, CH_2Cl_2, toluene, or THF. The average degree of polymerization (DP) for both polymers **4g** and **5g** was estimated using a combination of analytical SEC, ^{1}H NMR end-group analysis (assuming functionalization of both ends), and elemental analysis (EA). For D–D polymer **4g**, SEC, ^{1}H NMR end-group analysis, and EA afforded values for DP of ≈18, ≈15, and ≈12, respectively, whereas with ≈12, ≈12, and ≈10, slightly lower values were obtained for A–A polymer **5g**. Both **4g** and **5g** displayed a broad, asymmetric Gaussian-type molecular weight distribution in their MALDI-TOF-MS spectra (Figure 2). The most intense peak allowed a further estimate of the DP by means of mass spectrometry yielding for **4g** and **5g** values of ≈12 and ≈10, respectively. However, it has been reported that DP analysis by MALDI-TOF mass spectrometry might produce for some polymers misleading or even wrong results.[24]

The thermal stability of both polymers **4g** and **5g** was examined by conventional melting point (m.p.) determination and differential scanning calorimetry (DSC). They exhibited high thermal stability showing no sharp melting points, but started to decompose, accompanied by decoloration, at temperatures above 190 °C (**5g**) and 200 °C (**4g**), with continuing slow decomposition over a range of 50 °C and 35 °C, respectively.

As already observed for the terminally silyl substituted PTA oligomers **11 a–f**[7] and **3a–g**,[15, 16] D–D and A–A oligomers **4a–f** and **5a–f** proved to be remarkably stable under standard laboratory conditions. Their high solubility in a wide range of aprotic solvents such as $CHCl_3$, CH_2Cl_2, and THF enabled full analytical characterization by means of m.p., ^{1}H and ^{13}C NMR, FT-IR, Raman, UV/Vis spectroscopy, MALDI-TOF spectrometry, and EA. Whereas D–D substituted oligomers **4a–f** exhibited bright fluorescence in *n*-hexane and $CHCl_3$ solutions, which showed upon lengthening of the π-conjugated backbone a decrease in intensity, no fluorescence was observed for A–A functionalized compounds **5a–f**.

The molecular formula of each oligomer in series **4a–f** and **5a–f** was readily revealed by the MALDI-TOF mass spectra which depicted the molecular ions as parent ions. In addition, the number of monomeric units in each individual oligomer was also obtained by comparison of the ^{1}H NMR integrals of

0947-6539/00/0623-4402 $ 17.50+.50/0 *Chem. Eur. J.* **2000**, *6*, No. 23

the $Me_2tBuSiOCH_2$ resonances with those of the aromatic end-capping groups.

A pronounced difference was observed between the ^{13}C NMR spectra (125.8 MHz, $CDCl_3$) of the silyl-end-capped oligomeric PTA series **3a–g** and those of the functionalized derivatives **4a–f** and **5a–f**. In the silyl-end-capped series, the C(sp^2) and inner alkyne C(sp) resonances displayed signal overlap only at the stage of dodecamer **3f** and hexadecamer **3g**.[15, 16] In contrast, signal overlap in the D–D and A–A substituted oligomeric series already occurred at the stage of the pentamers. In the D–D series **4a–f**, the backbone C(sp^2) atom resonances for pentamer **4e** and hexamer **4f** showed peak overlap at $\delta = 132.8$, although C(sp) atom signals remained clearly separated even for the hexamer. For comparison, the polydisperse polymer **4g** displayed peak overlap for the backbone C(sp^2) resonances at $\delta = 132.3$. Peak overlapping was even more pronounced for the A–A series **5a–f**, with the inner C(sp) resonances already overlapping in pentamer **5e** at $\delta = 87.37$. Hexamer **5f** displays overlapping C(sp) resonances at $\delta = 87.38$ and 83.30 and backbone C(sp^2) resonances at $\delta = 132.43$. For comparison, the ^{13}C NMR resonances in the polydisperse A–A functionalized polymer **5g** merged at $\delta = 132.1$ [backbone C(sp^2)] and at $\delta = 87.1$ and 82.9 [C(sp)]. This analysis reveals a clear influence of the end-groups on the electronic properties of backbone C(sp) and C(sp^2) atoms in PTA oligomers. The data indicate that terminal substitution of PTA oligomers by either electron-releasing or -withdrawing groups results in a significant reduction of the oligomeric length at which individual carbon atoms start to resemble each other electronically. This observation is in agreement with similar findings from linear optical and Raman spectroscopical measurements (vide infra).

For comparison, we also prepared the D–A substituted dimer **12b** in addition to the known monomer **12a**.[17, 18] Oxidative coupling of **6** and **7** in a 1:1 ratio under Hay conditions provided a mixture of **4b** (22%):**12b** (12%):**5b** (24%) which was separated—quite tediously—by column and preparative thin-layer chromatography.

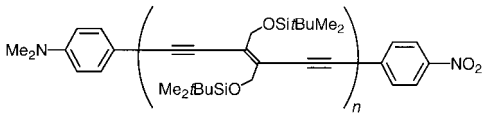

12a $n = 1$
12b $n = 2$

Electrochemistry: The redox characteristics of both series of end-functionalized oligomers and polymers, **4a–g** and **5a–g**, mono-functionalized monomers **9** and **10**, and D–A compounds **12a** and **12b** were investigated by a combination of cyclic (CV) and steady-state voltammetry (SSV) in CH_2Cl_2 using 0.1M nBu_4NPF_6 as supporting electrolyte (Table 1). For the 4-(dimethylamino)phenyl substituted compounds **4b–g**, **9**, and **12a–b**, the first observed oxidation potential occurred consistently at about +0.42 V versus Fc/Fc^+, which can be directly ascribed to the oxidation of the aniline group, as revealed by a direct comparison with *N*,*N*-dimethylaniline (cf. Table 1). Only for D–D monomer **4a**, a slightly lower oxidation potential of +0.31 V versus Fc/Fc^+ was observed. The reductions occurring on the DEE core for trimer **4c** and higher D–D functionalized oligomers were well-defined and behaved as quasi-reversible electron transfers as shown either by the slope of the wave in the steady-state voltammetry experiments or by the peak potential separation in the cyclic voltammograms.

Several discrete reduction steps were obtained for the A–A oligomers **5a–f**, for which the first one was reversible and involved a two-electron transfer. For compounds **5c–g**, one irreversible oxidation step was also observed between +1.30 V and +1.22 V versus Fc/Fc^+. This relatively high oxidation potential helps to account for the high environmental stability of these end-functionalized PTA oligomers. Whereas for all A–A functionalized oligomers **5a–f** the first reversible reductive electron transfer process occurred at −1.40 V versus Fc/Fc^+, the magnitude of the second reduction potential varied linearly with $1/n$. This result suggests that the first reduction occurred on both terminal 4-nitrophenyl groups, which could easily be verified by measuring reference compounds nitrobenzene and 4,4′-dinitrobiphenyl displaying reductions at −1.61 V and −1.44 V versus Fc/Fc^+, respectively. However, the peak potential difference observed by cyclic voltammetry and also the slope of the wave in the steady-state voltammetry experiments clearly indicated that the two one-electron reductions are not occurring at exactly the same potential. In fact, wave analysis revealed that the two one-electron reductions, occurring on the two terminal 4-nitrophenyl groups, are separated by about 50 mV.[25] This indicates that there is a certain degree of electronic communication between the 4-nitrophenyl end-groups and that these redox centers are not acting independently. It has been shown previously by spectroelectrochemistry that the first reduction step of **5a** occurs on the nitro groups generating a stable allenic dianion.[26]

The question whether both 4-nitrophenyl groups in **5a** undergo independent electrochemical reduction is of substantial interest. In a series of donor and/or acceptor functionalized tetraethynylethenes (TEEs, 3,4-diethynylhex-3-ene-1,5-diynes), the electrochemical results initially suggested that the π-conjugated carbon core is inefficient at delocalizing charges between the terminal redox centers, since the first redox potentials were essentially found to be independent of the substitution pattern about the TEE core and/or the presence of other functionalities.[26] However, comprehensive ab initio calculations on DEEs and TEEs revealed a much more complex mechanism of the redox process.[26]

With the exception of trimer **5c** and polydisperse A–A PTA polymer **5g**, for which a reversible second reduction was observed, the second reductive electron transfer steps in **5a–f** measured by CV were found to be irreversible. However, the observed slopes in the steady-state voltammetry for **5a–f** are in agreement with a quasi-reversible redox process, occurring on the DEE core. As expected, both D–D and A–A series **4c–f** and **5a–f** showed an increasingly facile first or second reduction potential upon lengthening of the π-conjugated

Table 1. Electrochemical data for D – D and A – A functionalized PTA oligomers and polymers **4a – g** and **5a – g**, monofunctionalized TEEs **9** and **10**, D – A functionalized oligomers **12a** and **12b**, and reference compounds aniline, nitrobenzene, and 4,4′-dinitrobiphenyl.

		cyclic voltammetry				steady-state voltammetry			
Compound	n	$E^{\prime\circ}$[a]	ΔE_p [mV][b]	E_{pc}[e]	E_{pa}[f]	$E_{1/2}^{red}$[g]	slope [mV][h]	$E_{1/2}^{ox}$[g]	slope [mV][h]
$PhNMe_2$	–	–	–	–	+0.44	–	–	+0.44	120
9	1	+0.40	88[c]		–	–	–	+0.41	73
4a	1	+0.31	85[c]	–	–	–	–	+0.32	82
4b	2	+0.41	74[d]	–	+0.99	–	–	+0.42	80
4c	3	−1.93	85	−2.19	+0.97	−1.96	86	+0.42	71
		+0.42	75			−2.18	89	+0.98	73
4d	4	−1.80	110	−2.02	+1.02	−1.88	88	+0.43	72
		+0.42	90			−2.01	80		
4e	5	−1.79	175	−2.37	–	−1.82	114	+0.43	69
		+0.43	80			−2.38	69		
4f	6	−1.74	130	−2.18	+1.02	−1.75	80	+0.42	65
		+0.42	75			−2.16	71		
4g	≈18	−1.70	125	–	–	−1.72	135	+0.41	73
		+0.41	95						
$PhNO_2$	–	−1.61	80	–	–	–	–	–	–
$(Ph\text{-}p\text{-}NO_2)_2$	–	−1.44	100	–	–	–	–[i]	–	–
10	1	−1.41	90	−2.00	–	−1.44	87	–	–
						−2.04	135		
5a	1	−1.42	120	−2.16	–	−1.45	100	–	–
						−2.12	180		
5b	2	−1.39	95	−1.90	–	−1.41	80	–	–
				−2.30		−1.87	80		
						−2.10	68		
5c	3	−1.39	95	–	+1.30	−1.40	80	+1.24	73
		−1.74	95			−1.79	92		
		−1.95	105			−1.94	100		
5d	4	−1.38	110	−1.73	+1.24	−1.39	85	+1.23	85
				−1.88		−1.78	110		
				−2.04		−2.20	100		
5e	5	−1.38	105	−1.79	+1.24	−1.40	90	+1.23	104
				−2.05		−1.74	65		
						−2.11	94		
5f	6	−1.38	100	−1.80	+1.22	−1.39	92	+1.19	109
				−1.93		−1.70	76		
						−1.98	148		
5g	≈12	−1.41	70	–	–	−1.37	135	+1.13	106
		−1.71	150			−1.69	78		
						−1.84	90		
12a	1	−1.43	80	−2.02	–	−1.43	73	+0.42	70
		+0.42	70[c]			−2.01	119		
12b	2	−1.40	85	−1.90	–	−1.43	66	+0.42	67
		+0.43	66[c]			−1.91	75		

[a] V versus Fc/Fc^+, redox potentials observed in CH_2Cl_2+0.1 M nBu_4NPF_6, scan rate $\nu = 100\ mV\,s^{-1}$, formal redox potential $E^{\prime\circ} = (E_{pa}+E_{pc})/2$. [b] $\Delta E_p = E_{ox} - E_{red}$, where subscripts ox and red refer to the conjugated oxidation and reduction steps, respectively. [c] Reversible electron transfer at scan rates $\nu = 200\ mV\,s^{-1}$. [d] Reversible electron transfer at scan rates $\nu = 1000\ mV\,s^{-1}$. [e] Peak potential E_{pc} for irreversible reduction. [f] Peak potential E_{pa} for irreversible oxidation. [g] V versus Fc/Fc^+, rotating disk electrode in CH_2Cl_2+0.1 M nBu_4NPF_6. [h] Logarithmic analysis of the wave obtained by plotting E versus $\log[I/(I_{lim} - I)]$. [i] Peak potential poorly resolved.

backbone. A plot of the reduction potentials versus $1/n$ for **4c – f** and **5a – f**, together with the corresponding higher polymers **4g** and **5g**, and the Me_3Si-end-capped oligomers **1a – f**, is provided in Figure 3. Upon extension of the central π-conjugated DEE core, both D – D oligomers **4c – f** and Me_3Si-end-capped series **1a – f** revealed a very similar slope of the first reduction potential as a function of the inverse number of monomer units. In contrast, a significantly different slope for the second reduction potential was obtained for the A – A series **5a – f**. The first reduction event occurs at the terminal 4-nitrophenyl groups at constant potential, whereas the second reduction event is located directly on the DEE core scaling linearly with $1/n$. In contrast to **1a – f** and **4c – f**, this reduction step takes place on a dianion and not on a neutral species. Surprisingly, this second reduction step for A – A series **5a – f** proved to be even more facile than the first reductive electron transfer of the silylated, neutral oligomers **1a – f**.[7] However, with increasing chain-length this effect vanishes and for both hexamers **4f** and **5f**, reduction was observed at nearly identical potentials, indicating that at longer chain-lengths the position of the electron transfer potential associated with the conjugated backbone is no longer influenced by the nature of the end-groups. This striking observation strongly suggests that PTA oligomers bearing terminal 4-nitrophenyl anions still display electron-acceptor properties, although certainly not as strong as in their

0947-6539/00/0623-4404 $ 17.50+.50/0 *Chem. Eur. J.* **2000**, *6*, No. 23

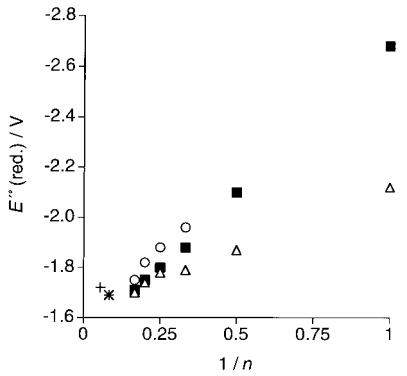

Figure 3. Evolution of the first reduction potentials of Me_3Si-end-capped oligomers **1b–f** (CV, ■), D–D compounds **4c–f** (SSV, ○), the second reduction potentials of A–A oligomers **5a–f** (SSV, △) recorded in CH_2Cl_2 (0.1M nBu_4NPF_6, V vs. Fc/Fc^+), and monomer **1a** (CV, filled square) in THF plotted as a function of $1/n$. Included are also the reduction potentials for D–D and A–A polymers **4g** (SSV, +) and **5g** (SSV, *), respectively.

neutral form. However, it should be noted that in the case of the silylated oligomers **1a–f** the first electron transfer event is reversible, whereas for A–A oligomers **5a–f** the reduction located at the DEE backbone is not. Surprisingly, unfavorable Coulombic interactions resulting from a third electron on the π-conjugated core of the A–A oligomer dianions still seem to be outweighed by the electron-stabilizing properties of the 4-nitrophenyl groups. This astonishing experimental observation might be explained by the presence of strongly localized charge carriers on the nitro groups which, in addition, could adopt a perpendicular orientation with respect to the preferentially planar[27] arylated PTA backbone, thus reducing repulsive destabilizing interactions.

All three D–D-, A–A-, and Me_3Si-end-capped oligomer series merged at the same averaged reduction potential of -1.70 V versus Fc/Fc^+, including polymers **4g** and **5g**. Despite the fact that for the two bis-functionalized polymers saturation for the reduction potential was attained, the redox activity of the end-groups still remained clearly detectable. The reduction potential of $E_{red} = -1.70$ V versus Fc/Fc^+ for an infinitely long PTA chain is in full agreement with the previously experimentally derived value utilizing the Et_3Si-end-capped oligomer series **3a–g**.[16] Linear optical spectroscopy in $CHCl_3$ solutions revealed for the transition energy of the deconvoluted longest-wavelength absorption band λ_{max} of dodecamer **3f** a value of $E_{max} = 2.63$ eV.[15, 16] For A–A PTA polymer **5g**, a very similar value of $\Delta E = 2.50$ eV was deduced from steady-state voltammetry measurements. In addition, analysis of the reduction potentials versus $1/n$ for both functionalized series **4a–g** and **5a–g** allows also a rough estimation of the ECL which yields $n \approx 10$ monomer units, independent of the nature of the end-groups.

However, this estimate of the ECL relies very strongly on the experimental accuracy of the reduction potentials. Even the slightest deviations in the second decimal place of the reduction potentials have considerable influence on the slope of the line obtained by linear regression. For both substituted PTA series **4a–f** and **5a–f**, the SSV data were found to follow more closely a linear relationship between reduction potential and inverse number of monomer units than the data obtained from CV measurements.

Linear evolution of redox potentials with the inverse number of monomer units has also been reported for other conjugated oligomer systems such as oligo(α-thiophene)s,[28] oligo(α-thiophene vinylene)s,[29] or oligo(*p*-phenylene vinylene)s.[30]

Linear optical properties: The UV/Vis spectra of end-functionalized PTA oligomers **4a–f** and **5a–f**, and the corresponding polydisperse polymers **4g** and **5g** were recorded in $CHCl_3$ solutions at 20 °C (Figure 4). As already reported

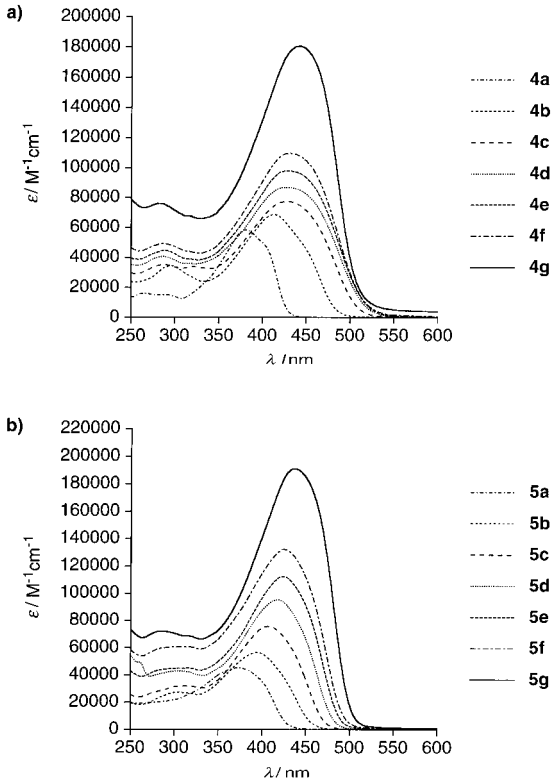

Figure 4. Electronic absorption spectra of a) D–D substituted **4a–g** and b) A–A substituted **5a–g** in $CHCl_3$ at 20 °C.

for the silyl-end-capped oligomeric series **1a–f** and **3a–g**, a bathochromic shift of the longest-wavelength absorption maximum λ_{max} upon extension of the conjugated carbon backbone was observed, and to a first approximation the molar extinction coefficients ε increased proportionally to the number of monomer units.[7, 15, 16] Owing to the inhomogeneously broadened longest-wavelength absorption bands in both series **4a–g** and **5a–g**, accurate determination of the λ_{max} and E_{max} values required deconvolution of the absorption spectra;[7] the obtained λ_{max} and E_{max} values are listed in Table 2. The most striking difference between the two functionalized PTA series lies in the much earlier saturation of λ_{max} versus n of the D–D substituted oligomers **4a–f** compared with their A–A functionalized counterparts **5a–f**. Whereas in the D–D series, no additional increase for λ_{max} in going from tetramer **4e** to pentamer **4f** was observed, no such early saturation was obtained for the A–A series **5a–f** (Figure 5). Thus, the ECL derived from UV/Vis data for

Table 2. UV/Vis data of D–D and A–A functionalized PTA oligomers **4a–f** and **5a–f**, polymers **4g** and **5g**, monofunctionalized monomers **9** and **10**, and D–A compounds **12a** and **12b**.

Compound	n	λ_{max} [nm] (eV) [a] ε [$M^{-1}cm^{-1}$][b]	Compound	n	λ_{max} [nm] (eV)[a] ε [$M^{-1}cm^{-1}$][b]
9	1	379.1 ± 0.1 (3.27) 30600	**10**	1	376.6 ± 1.6 (3.29) 17100
4a	1	408.6 ± 0.1 (3.03) 41500	**5a**	1	402.9 ± 0.5 (3.08) 27600
4b	2	454.8 ± 0.3 (2.72) 42600	**5b**	2	430.4 ± 0.3 (2.88) 33100
4c	3	469.3 ± 0.7 (2.64) 53900	**5c**	3	442.5 ± 0.7 (2.80) 47900
4d	4	472.0 ± 1.9 (2.62) 64200	**5d**	4	455.2 ± 0.6 (2.72) 57300
4e	5	472.4 ± 1.2 (2.62) 73000	**5e**	5	460.9 ± 0.7 (2.69) 70000
4f	6	472.4 ± 1.1 (2.62) 81000	**5f**	6	464.2 ± 0.8 (2.67) 83000
4g	≈18	472.4 ± 0.8 (2.62) 146300[c]	**5g**	≈12	470.2 ± 0.6 (2.63) 146800[c]
12a	1	450.4 ± 0.9 (2.75) 20400	**12b**	2	456.4 ± 0.5 (2.71) 32100

[a] Longest-wavelength absorption maximum in $CHCl_3$ at 20 °C, obtained by deconvolution of the absorption spectra.[7] [b] Molar extinction coefficient. [c] Molar extinction coefficient based on the average polymerization degree derived from analytical SEC.

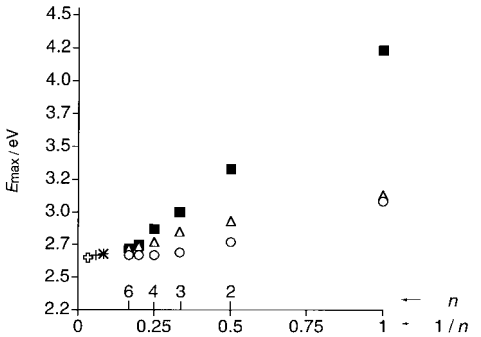

Figure 5. Graphical representation of the longest-wavelength transition energies E_{max} obtained by deconvolution for D–D and A–A substituted oligomers **4a–f** (○) and **5a–f** (△), Me_3Si-end-capped oligomer series **1a–f** (■), as well as the corresponding polydisperse polymers **4g** (+), **5g** (*), and **2b** (✠), respectively.

the D–D series **4a–f** can be estimated to $n = 4$ monomer units. In a similar procedure, assuming that saturation of the linear optical properties is already attained for the A–A functionalized polymer **5g**, the ECL can be estimated to about $n = 10$ monomer units. This value is considerably larger than the one for D–D series **4a–f**, but in agreement with the previous ECL data for the silyl-end-capped series **1a–f**[7] and **3a–g**.[15, 16] Interestingly, the UV/Vis derived ECL for D–D oligomers **4a–f** contrasts with the electrochemical results, which did not indicate saturation at such a short chain-length.

Previous electrochemical measurements revealed that diethynylethenes such as **1a** and **3a** possess substantial electron-accepting properties,[31] which helps to explain the linear optical trends observed for the two end-functionalized series **4a–f** and **5a–f** in this study. In the case of A–A oligomers **5a–f**, the terminal 4-nitrobenzene groups do not seem to be capable of creating a noticeable internal charge-transfer (CT). Thus, the evolution of the optical properties as a function of the chain-length is only marginally influenced, and the ECL is found to be in the range of $n = 10$ monomer units as previously estimated for the parent series **1a–f**.[7] In contrast, the 4-(dimethylamino)-phenyl end-groups of D–D series **4a–f** are strong electron-donors leading to an intramolecular CT transition between the terminal electron-donating and the internal electron-accepting DEE backbone, ultimately dominating the linear optical properties. These internal CT transitions are strongly localized and are hardly affected by an increase of the conjugated π-system, which explains the experimentally observed early saturation of λ_{max} at the stage of tetramer **4d**.

Of all three series **1a–f**, **4a–f**, and **5a–f** investigated, the Me_3Si-end-capped oligomers **1a–f** displayed the largest relative total bathochromic shift $\Delta\lambda_{max}$ in going from monomer to polymer, whereas D–D and A–A functionalized oligomers revealed a much smaller disparity in their λ_{max} values (Figure 5). Interestingly, the type of end-substitution, may it be either electron-releasing or -withdrawing, showed a minimal effect on λ_{max} for monomers **4a** and **5a** as reflected by the very similar values of 409 and 403 nm, respectively (Table 2). Conversely, aryl-end-substitution in **4a** and **5a** resulted in a significant bathochromic shift for λ_{max} of 110 nm compared with the bis-silylated monomer **1a**. However, Figure 5 clearly shows that all three series converge at higher oligomer lengths and the three differently substituted polydisperse polymers **2b**, **4g**, and **5g** ultimately converge at the same longest-wavelength absorption maxima of $\lambda_{max} \approx 470$ nm ($E_{max} \approx 2.6$ eV), providing evidence that with increasing chain-length the influence of the terminal substituents decreases and, above the ECL, entirely vanishes.

The UV/Vis spectrum of D–A substituted monomer **12a** exhibited a broad absorption band, which is bathochromically shifted compared with the λ_{max} of symmetrically D–D and A–A substituted monomers **4a** and **5a** (Table 2). The end-absorption of this band extends beyond 500 nm, which is indicative of an intramolecular CT transition. Whereas the D–D and D–A compounds **4b** and **12b** exhibited with 455 and 456 nm nearly identical λ_{max} values, the longest-wavelength absorption for A–A dimer **5b** was hypsochromically shifted to 430 nm (Table 2). As expected, the effect of the intramolecular CT on the shape and position of the absorption bands of D–A dimer **12b** was not as pronounced as in the case of monomeric **12a**. In addition, increase of the linear conjugation pathway resulted in a rather modest bathochromic shift of the CT band in going from monomer **12a** ($\lambda_{max} =$ 450 nm) to dimer **12b** ($\lambda_{max} = 456$ nm) (Table 2).

0947-6539/00/0623-4406 $ 17.50+.50/0 *Chem. Eur. J.* **2000**, *6*, No. 23

Raman scattering studies: Raman spectroscopy of D–D and A–A substituted oligomers **4a–f** and **5a–f** was performed in $CHCl_3$ solutions at 20 °C. As observed for the silylated series **1a–f** and **3a–f**,[15, 16] the frequencies of the Raman-active stretches of both double and triple bonds, $\tilde{\nu}_{(C=C)}$ and $\tilde{\nu}_{(C\equiv C)}$, decreased upon lengthening of the π-conjugated chain (Table 3). Whereas for the C–C triple bond stretches $\tilde{\nu}_{(C\equiv C)}$ sharp absorption bands were obtained, the olefinic bonds for the D–D and A–A substituted PTA oligomers **4a–f** and **5a–f** gave raise to numerous weak and ill-defined absorption bands, possibly owing to the additional aryl end-groups. Therefore, the following discussion will only focus on the Raman-active $\tilde{\nu}_{(C\equiv C)}$ stretches. In general, the Raman resonance frequencies for the C–C triple bonds varied in going from monomer to polymer for both functionalized series **4a–f** and **5a–f** (e.g. **5a**: 2179 cm^{-1}, **5g**: 2158 cm^{-1}) over a much smaller range than for the parent Me_3Si-end-capped PTA oligomers **1a–f** (**1a**: 2213 cm^{-1}, **2a**: 2156 cm^{-1}). In addition, D–D series **4a–f** showed the smallest changes of $\Delta\tilde{\nu}_{(C\equiv C)}$ between successive oligomers and saturation of the resonance frequency $\tilde{\nu}_{(C\equiv C)}$ was already obtained for trimer **4c** (2156 cm^{-1}), which parallels the findings from linear optical spectroscopy (see above). A plot of the experimentally obtained $\tilde{\nu}_{(C\equiv C)}$ Raman frequencies as a function of the number of monomer units for the two series **4a–f** and **5a–f** is given in Figure 6. For comparison, the Raman frequencies of Me_3Si-end-capped oligomers **1a–f**, polymers **2a**, **4g**, and **5g** are also included.

Table 3. Raman scattering data of oligomers **1a–f**, **4a–f**, and **5a–f** and polymers **2a**, **4g**, and **5g**.

Compound	n	$\tilde{\nu}_{(C\equiv C)}$ [cm^{-1}][a]	Compound	n	$\tilde{\nu}_{(C+C)}$ [cm^{-1}][a]	Compound	n	$\tilde{\nu}_{(C\equiv C)}$ [cm^{-1}][a]
1a	1	2213	**4a**	1	2162	**5a**	1	2179
1b	2	2187	**4b**	2	2158	**5b**	2	2170
1c	3	2175	**4c**	3	2156	**5c**	3	2166
1d	4	2169	**4d**	4	2156	**5d**	4	2164
1e	5	2165	**4e**	5	2156	**5e**	5	2163
1f	6	2163	**4f**	6	2156	**5f**	6	2162
2a	≈22	2156	**4g**	≈18	2156	**5g**	≈12	2158

[a] Raman frequencies measured in $CHCl_3$ solutions at 20 °C.

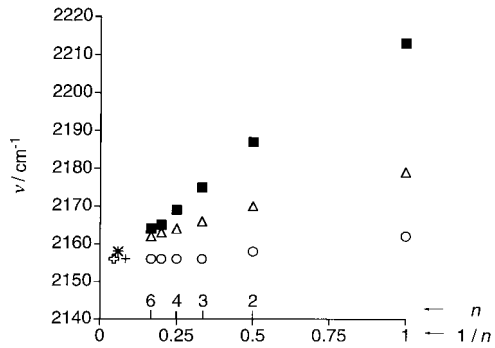

Figure 6. Comparative plot of the Raman-active stretches $\tilde{\nu}_{(C\equiv C)}$ for Me_3Si-end-capped oligomers **1a–f** (■), D–D compounds **4a–f** (○), and A–A oligomers **5a–f** (△) recorded in $CHCl_3$ solutions. Included are also the values for polymer **2a** (⊕), and D–D and A–A polymers **4g** (+) and **5g** (*), respectively.

To a first approximation, a linear correlation between the $\tilde{\nu}_{(C\equiv C)}$ Raman shifts and the inverse number of monomer units is observed, although for the D–D series this holds only true for monomer **4a** to trimer **4c**. All three series converge at $\tilde{\nu}_{(C\equiv C)} = 2156\ cm^{-1}$, showing only for polymer **4g** a slightly higher value of 2158 cm^{-1}. Crossing of the linear regression line through the data points obtained for Me_3Si-end-capped oligomers **1a–f** and A–A oligomers **5a–f** with the horizontal saturation line of polymers **2a** and **5g** (intercepting the y axis at an averaged value of 2157 cm^{-1}) yields an ECL of about $n = 10$ monomer units, which is in good agreement with the results obtained from UV/Vis spectroscopy.

Nonlinear optical properties: The second hyperpolarizability γ of the D–D and A–A arylated PTA oligomers **4a–f** and **5a–f**, the corresponding polymers **4g** and **5g**, the mono-functionalized monomers **9** and **10**, as well as the D–A systems **12a** and **12b** were measured by a combination of third-harmonic generation (THG) and degenerate four-wave mixing (DFWM) in $CHCl_3$ solutions (Table 4). With the exception of tetramer **4d**, pentamers **4e**, **5e**, hexamers **4f**, **5f**, and polymers **4g** and **5g**, which showed slight absorption at the third-harmonic frequency 3ω (636 nm), none of the other compounds investigated absorbed at this wavelength and thus their γ values are not resonantly enhanced. The microscopic hyperpolarizability γ values were then transformed to the macroscopic hyperpolarizability $\chi^{(3)}_{100\,\%}$ by assuming an isotropic arrangement of the molecules, using the density and refractive indices (for local field corrections) of the solvent $CHCl_3$, to give a lower limit of what can be expected in the bulk sample.

The experimental results listed in Table 4 lead to a number of very interesting and also astonishing conclusions. Firstly, bis-substitution with electron-releasing or electron-accepting groups significantly increased the nonlinearity (by up to 14 times) compared with the corresponding bis-end-silylated DEEs. Similar observations had also been made for TEEs[32] and other classes of NLO chromophores.[33] Interestingly, the 4-(dimethylamino)phenyl donor group in mono-arylated DEE **9** was not found to enhance the second hyperpolarizability γ or $\chi^{(3)}_{100\,\%}$ in contrast to mono-nitro functionalized **10**, and both compounds gave identical values. In addition, the donor groups in monomer **4a** enhanced γ by a factor of only 1.4 compared with the corresponding acceptor DEE **5a** (Figure 7). In contrast, the effect of the 4-(dimethylamino)-phenyl donor groups in similar TEE derivatives led to a two-fold increase of the nonlinear optical response, probably owing to the stronger acceptor properties of TEEs.[32]

Secondly, an up to 28-fold increase in the value of γ was obtained by changing from centrosymmetric unsubstituted DEEs to acentric D–A functionalization (**1a**: $\gamma = 9.2 \times 10^{-36}$ esu;[34] **12a**: $\gamma = 250 \times 10^{-36}$ esu). Changing from symmetrical D–D or A–A substitution to acentric D–A systems

Table 4. Second hyperpolarizability data of D–D and A–A functionalized PTA oligomers **4a–f** and **5a–f**, polymers **4g** and **5g**, monofunctionalized oligomers **9** and **10**, and D–A compounds **12a** and **12b**. For comparison, the values of polymers **2a** and **2b** are also included. The THG experiments were performed at a fundamental wavelength of $\lambda = 1907$ nm and the DFWM measurements at a wavelength of $\lambda = 1047$ nm.[a]

Compound	n	$\varepsilon_{3\omega}$ [M^{-1} cm^{-1}]	γ_{THG} [10^{-36} esu]	γ_{THG} [10^{-48} m^5 V^{-2}]	γ_{DFWM} [10^{-36} esu]	γ_{DFWM} [10^{-48} m^5 V^{-2}]
2a	±22	410	6500	91	7500	105
2b	±31	0	9200	129	–	–
4a	1	0	123	1.72	320	4.4
4b	2	16	430	6.0	–	–
4c	3	36	740	10.4	2000	28
4d	4	96	1320	18.4	2700	38
4e	5	100	1480	20.6	4000	56
4f	6	198	1200	16.8	4300	61
4g	≈18	550	6000	84	10500	146
5a	1	0	88	1.23	230	3.2
5b	2	0	220	3.1	420	5.9
5c	3	19	460	6.4	740	10.4
5d	4	31	720	10	1370	19
5e	5	65	880	12	1600	22
5f	6	104	920	13	1440	20
5g	≈12	380	3700	52	5000	70
9	1	0	51	0.71	–	–
10	1	0	51	0.71	–	–
12a	1	0	250	3.5	–	–
12b	2	4	465	6.5	1010	14.1

[a] Reference $\chi^{(3)}_{fs} = 1.6 \times 10^{-22}$ m^2 V^{-2}, $\chi^{(3)}_{Cs_2} = 3.0 \times 10^{-20}$ m^2 V^{-2}, experimental error 10% for THG and 15% for DFWM.

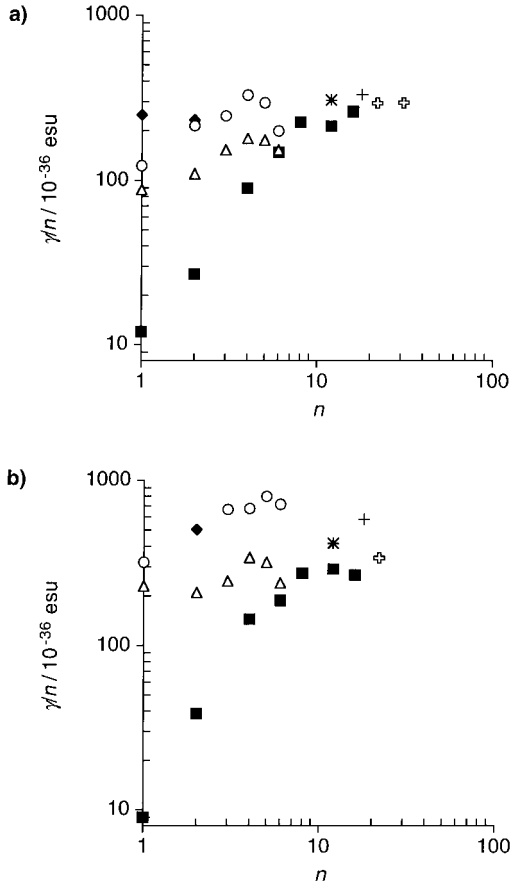

Figure 7. Double logarithmic plot of the second hyperpolarizability γ per monomer unit of Et_3Si-end-capped oligomers **3a–g** (■), D–D oligomers **4a–f** (○), A–A oligomers **5a–f** (△), D–A compounds **12a**,**b** (◆), silyl-end-capped polymers **2a**,**b** (⊕), and D–D and A–A polymers **4g** (+) and **5g** (*), respectively, versus the number of monomer units n measured a) by THG and b) by DFWM.

still resulted in a two-fold increase in γ (**4a**: $\gamma = 123 \times 10^{-36}$ esu; **12a**: $\gamma = 250 \times 10^{-36}$ esu). These experiments are in agreement with previous results obtained for TEEs[32] and Et_3Si-end-capped DEE oligomers **3a–f**[16, 35] as well as theoretical predictions by Garito et al.[36] and the widely used three-level model for γ derived from static perturbation theory.[37] The beneficial effect of asymmetrical electron distribution on γ vanished almost completely in D–A dimer **12b**, which only showed a minor enhanced value compared with the corresponding symmetrically substituted D–D oligomer **4b**.

Thirdly, an increase in conjugation length resulted in larger values of γ. This is illustrated by both functionalized series **4a–f** and **5a–f** and is in full agreement with the data collected for the two doubly end-silylated oligomer series **1a–f**[7] and **3a–f**[16, 35] (Figure 7).

As expected, both symmetrically functionalized monomers **4a** and **5a** displayed significantly higher γ values than the parent DEE monomers **1a** and **3a**. Interestingly, the higher oligomers of all three series approach the saturation values measured for the polydisperse PTA polymers **2a** and **2b**, which can be viewed as samples of an infinitely long PTA backbone. Although the two D–D and A–A substituted polymers **4g** and **5g** match the saturation values of PTAs **2a** and **2b**, the influence of D–D and A–A end-functionalization in enhancing the third-order nonlinear optical response was clearly detectable up to hexamers **4f** and **5f**, which still displayed significantly larger γ values compared with the parent Et_3Si-end-capped hexamer **3d**. A double logarithmic plot of γ/n versus n revealed that the bis-end-silylated oligomer series **3a–d** featured a much steeper increase of γ/n than observed for both arylated oligomer series **4a–f** and **5a–f** (Figure 7). Interestingly, both **4a–f** and **5a–f** displayed a sigmoidal relationship between γ/n and the number of monomer units similar to that observed for the end-silylated oligomer series. The fact that our DFWM experiments of the D–D and A–A functionalized PTA oligomers yielded larger nonlinearities than for the corresponding silyl-end-capped ones can be explained by the closeness of the two-photon resonance.

The chain-length dependence of γ/n displayed a rather unusual picture for both functionalized series. The γ/n values for the higher oligomers not only leveled off but reached for tetramers **4d** and **5d** a maximum value and decreased again for the corresponding pentamers and hexamers. Surprisingly, the γ/n values of hexamers **4f** and **5f** even dropped below those obtained for trimers **4c** and **5c**, respectively. The possibility that the observed deviations arised from decom-

0947-6539/00/0623-4408 $ 17.50+.50/0 *Chem. Eur. J.* **2000**, *6*, No. 23

positions occurring during the THG measurements was discounted by analytical controls (UV/Vis and analytical SEC) immediately after laser irradiation, which showed no indication of photochemical instability. The values for polydisperse polymers **4g** and **5g** converged at a similar value obtained for PTAs **2a** and **2b**. The fact that exactly the same trend, although not in such a pronounced form, was observed for the parent PTA series **3a–f** strongly indicates, that this behavior is certainly not coincidental but has a physical meaning, yet to be theoretically analyzed. It appears, that the influence of the terminally functionalized aryl groups on γ/n lasts only a few monomer units and nearly vanishes at the stage of the pentamers/hexamers to be then dominated by the nonlinear response of the PTA backbone itself. For the bis-end-silylated oligomers **3a–f** this feature is much less pronounced, possibly owing to the weak electron-donating effect of trialkylsilyl groups. It is becoming clear from the comprehensive set of data (Table 4, Figure 7) that the relationship between second hyperpolarizability and chain-length in a given class of π-conjugated oligomers may be substantially more complex than initially anticipated and may not necessarily follow the widely accepted three-level model for γ. Only a combination of theoretical and experimental investigations will be able to provide the information needed for developing a clearer picture of the underlying physics.

Conclusion

The study of the influence of terminal electron-releasing [4-(dimethylamino)phenyl] and -withdrawing (4-nitrophenyl) substituents on the PTA backbone as a function of chain-length has provided further insight into the electronic characteristics of this class of π-conjugated polymers. The donor substituted oligomers showed for the oxidation of the aniline groups a constant first reversible oxidation potential around $+0.42$ V versus Fc/Fc^+, and with the exception of monomer and pentamer, a second irreversible oxidation event was observed around $+1.00$ V versus Fc/Fc^+. In contrast, the 4-nitrophenyl functionalized systems starting with the trimer gave only one irreversible oxidation (of the DEE core) at about $+1.24$ V versus Fc/Fc^+. In addition, all oligomers bearing two acceptor groups displayed a reversible two-electron reduction event at -1.40 V versus Fc/Fc^+. In accordance with Me_3Si- and Et_3Si-end-capped PTA oligomers, both D–D and A–A functionalized series revealed an increasingly facile first or second reduction step upon elongation of the π-conjugated backbone. A plot of the reduction potential versus the inverse number of monomer units for both D–D and A–A functionalized series displayed independently of the nature of terminal functionalization saturation for the electron transfer around $n \approx 10$ monomer units. Interestingly, the second reduction step of the A–A oligomers, which takes place on a dianion, was found to be even more facile than the first reductive electron transfer on the neutral Me_3Si-end-capped oligomers. This observation suggests that 4-nitrophenyl radical anions still exhibit significant electron-accepting properties.

The effective conjugation length estimated from the deconvoluted longest-wavelength absorption maxima for the A–A oligomer series was found to be on the order of $n = 10$ monomer units and thus in accord with results obtained for the silyl-end-capped PTA oligomers. In contrast, a significantly reduced ECL with $n = 4$ was obtained for the D–D series, probably owing to the formation of strong CT bands dominating the absorption properties. Raman scattering measurements revealed with $n = 3$ for the latter series an even more reduced value for the ECL.

Significant increases for the second hyperpolarizability γ upon terminal substitution with donor and acceptor groups were found by THG as well as DFWM. However, the chain-length dependence of γ/n revealed for both substituted series a rather unusual result. The γ/n values of the higher oligomers in both functionalized series did not only level off but reached with their tetramers a maximum value and then dropped drastically for the corresponding pentamers and hexamers. This effect was found to be independent on the nature of the end-groups and was considerably more pronounced than in the case of the terminally silylated higher oligomers. Interestingly, THG experiments showed that the hyperpolarizabilities for long PTA oligomers reach the same saturation values as their unsubstituted counterparts.

This comprehensive investigation of end-functionalized PTA oligomers clearly shows that the influence of the terminal groups on physical effects involving the entire π-conjugated framework vanishes upon passing from oligomers to longer-chain polymers. On the contrary, physical events such as electron transfers specifically located at the terminal arylated end-groups remain constant or are minimally influenced upon lengthening of the π-conjugated backbone.

Experimental Section

Materials and general methods: See ref. [16] for full details. Compounds **4a**, **6**, **8**, **9**, **12a**,[17, 18] **5a**,[20] and **11**[21, 22] were prepared as previously described. The ^{13}C NMR spectra of polymers **4g** and **5g** were recorded using $Cr(acac)_3$ (≈20 mM) as a relaxation agent. Resonances of the $Me_2tBuSiOCH_2$-side-chain in **4b–f** and **5b–f** frequently give rise to signal overlap whereas, apart from compounds **4e–g** and **5e–g**, the ^{13}C NMR resonances of the conjugated backbone were always clearly distinguishable. MALDI-TOF-MS spectra were obtained using a Bruker Reflex instrument with a N_2 laser system (337 nm) to desorb and ionize analyte molecules, which were previously dissolved in CH_2Cl_2 and deposited onto the center of the probe tip and dried under vacuum. 3-(3-Indolyl)acrylic acid (IAA) or 2′,4′,6′-trihydroxyacetophenone (THA)/ammonium hydrogen citrate (AHC) were used as matrices. All reported data were acquired using the linear positive-ion mode at +15 and 20 kV, respectively. For EI, FAB, and MALDI-TOF mass spectra of all monomers and oligomers, the experimental highest peak in the molecular ion cluster is reported followed in parenthesis by the isotopic molecular formula corresponding to the calculated most intense peak in the cluster.

Analytical size-exclusion chromatography (SEC): see ref. [16] for full details. Molecular weight determinations of polymers **4g** and **5g**: Columns: Polymer Laboratories PL-Gel mixed-C5 (5 μm), 7.5 mm ID × 60 cm. Instrumentation: Knauer gel permeation chromatograph equipped with a KMX-6-LAALS-detector (low angle laser light scattering) from Chromatix and a Viscotek-differential-viscosimeter H502. Data aquisition and evaluation: software program TriSEC GPC-Software (Version 2.7); solvent THF (HPLC grade) thermostatted at 45 °C; flow rate fixed at 1 mL min^{-1}. Calibration with polystyrene standards from Polymer Laboratories.

Preparative size-exclusion chromatography (SEC), **electrochemistry measurements**, **third-harmonic generation measurements**, and **degenerate four-wave mixing experiments**: see refs. [16, 35] for full details.

D–D oligomers 4b–f and polymer 4g: TMEDA (0.031 g, 0.04 mL, 0.27 mmol) and CuCl (0.008 g, 0.081 mmol) were added at 20 °C to a

solution of **6** (0.138 g, 0.29 mmol) and **11** (0.035 g, 0.095 mmol) in dry CH_2Cl_2 (10 mL, containing 4 Å molecular sieves). After the reaction mixture was stirred in air for 2 h, an EDTA (ethylenediaminetetraacidic acid) solution (pH 8, 100 mL) was added and the reaction mixture extracted with CH_2Cl_2 until the washings were colorless. The organic phase was washed with saturated aqueous K_2CO_3 solution (50 mL) and dried ($MgSO_4$). Concentration in vacuo (at water aspirator pressure), purification by size-exclusion chromatography, and precipitation from MeOH gave the D–D oligomers **4b–f** and polymer **4g** as solids.

(*E*,*E*)-3,4,9,10-Tetrakis{[(*tert*-butyl)dimethylsilyloxy]methyl}-1,12-bis[4-(dimethylamino)phenyl]dodeca-3,9-diene-1,5,7,11-tetrayne (4b): Orange solid (0.086 g, 62%); m.p. 154–155 °C (lit. 153–155 °C[17, 18]); ^{1}H NMR (500 MHz, $CDCl_3$): $\delta = 0.11$ (s, 12H), 0.12 (s, 12H), 0.915 (s, 18H), 0.920 (s, 18H), 2.98 (s, 12H), 4.51 (s, 4H), 4.55 (s, 4H), 6.62 (d, $J = 8.9$ Hz, 4H), 7.30 (d, $J = 8.9$ Hz, 4H); ^{13}C NMR (125.8 MHz, $CDCl_3$): $\delta = -5.06$, 18.42, 18.44, 25.96, 40.13, 63.98, 64.33, 82.64, 85.07, 85.56, 105.26, 109.88, 111.75, 126.21, 132.73, 133.95, 150.36; Raman ($CHCl_3$): $\tilde{\nu} = 2925$ (w = weak), 2398 (w), 2158 (m = medium), 1606 (w), 1562 (w), 1519 (w), 1372 (w), 1214 (m), 1155 (w), 973 (w), 761 (m), 665 (s = strong), 364 (s), 259 (s) cm^{-1}; MALDI-TOF-MS (THA, AHC): *m*/*z* (%): 987.8 (45, $[M+Na]^+$), 965.5 (100, $[M]^+$; calcd $^{12}C_{55}{}^{13}CH_{88}N_2O_4{}^{28}Si_4{}^+$: 965.6), 907.5 (9, $[M-C(CH_3)_3]^+$), 833.8 (67, $[M-OSi(CH_3)_2C(CH_3)_3]^+$).

(*E*,*E*,*E*)-3,4,9,10,15,16-Hexakis{[(*tert*-butyl)dimethylsilyloxy]methyl}-1,18-bis[4-(dimethylamino)phenyl]octadeca-3,9,15-triene-1,5,7,11,13,17-hexayne (4c): Orange solid (0.034 g, 18%); m.p. >170 °C (decoloration from orange to deep red), 203–206 °C (melt.); ^{1}H NMR (500 MHz, $CDCl_3$): $\delta =$ 0.102 (s, 12H), 0.105 (s, 12H), 0.117 (s, 12H), 0.910 (s, 18H), 0.911 (s, 18H), 0.919 (s, 18H), 2.98 (s, 12H), 4.46 (s, 4H), 4.50 (s, 4H), 4.55 (s, 4H), 6.62 (d, $J = 9.0$ Hz, 4H), 7.31 (d, $J = 9.0$ Hz, 4H); ^{13}C NMR (125.8 MHz, $CDCl_3$): $\delta = -5.13$, -5.08, -5.07, 18.37, 18.41, 18.43, 25.90, 25.95, 40.12, 63.91, 63.95, 64.32, 81.75, 84.26, 84.58, 85.57, 87.73, 105.77, 109.74, 111.74, 125.89, 132.01, 132.78, 134.60, 150.42; FT-IR ($CHCl_3$): $\tilde{\nu} = 3011$ (m), 2956 (m), 2933 (m), 2856 (m), 2400 (m), 2167 (w), 1606 (s), 1522 (m), 1445 (m), 1361 (m), 1267 (s), 1111 (m), 1045 (w), 1006 (w), 933 (w), 839 (s) cm^{-1}; Raman ($CHCl_3$): $\tilde{\nu} = 2925$ (w), 2399 (w), 2156 (m), 1605 (w), 1558 (m), 1372 (w), 1214 (m), 1149 (w), 971 (w), 762 (m), 665 (s), 364 (s), 259 (s) cm^{-1}; UV/Vis ($CHCl_3$): $\lambda = 288$ (35400), 320 (33900), 427 (77500); MALDI-TOF-MS (THA, AHC): *m*/*z* (%): 1352.1 (28, $[M+Na]^+$), 1328.5 (100, $[M]^+$; calcd $^{12}C_{75}{}^{13}CH_{122}N_2O_6{}^{28}Si_6{}^+$: 1327.8), 1271.2 (41, $[M-C(CH_3)_3]^+$), 1197.0 (43, $[M-OSi(CH_3)_2C(CH_3)_3]^+$); $C_{76}H_{122}N_2O_6Si_6$ (1328.34): calcd C 68.72, H 9.26, N 2.11; found: C 68.68, H 9.26, N 2.09.

(*E*,*E*,*E*,*E*)-3,4,9,10,15,16,21,22-Octakis{[(*tert*-butyl)dimethylsilyloxy]methyl}-1,24-bis[4-(dimethylamino)phenyl]tetracosa-3,9,15,21-tetraene-1,5,7,11,13,17,19,23-octayne (4d): Deep orange solid (0.017 g, 7%); m.p. >190 °C (decoloration from red to deep red), 220–224 °C (decomp.); ^{1}H NMR (500 MHz, $CDCl_3$): $\delta = 0.093$ (s, 12H), 0.096 (s, 12H), 0.102 (s, 12H), 0.115 (s, 12H), 0.903 (s, 18H), 0.906 (s, 18H), 0.909 (s, 18H), 0.916 (s, 18H), 2.98 (s, 12H), 4.445–4.446 (overlap, 4H), 4.451–4.453 (overlap, 4H), 4.49 (s, 4H), 4.55 (s, 4H), 6.62 (d, $J = 9.0$ Hz, 4H), 7.30 (d, $J = 9.0$ Hz, 4H); ^{13}C NMR (125.8 MHz, $CDCl_3$): $\delta = -5.14$, -5.08, -5.07, 18.36, 18.37, 18.41, 18.43, 25.89, 25.95, 40.12, 63.88, 63.90, 63.95, 64.32, 81.59, 83.20, 84.49, 84.52, 85.57, 87.11, 88.09, 105.88, 109.71, 111.74, 125.82, 131.69, 132.65, 132.79, 134.74, 150.44; FT-IR ($CHCl_3$): $\tilde{\nu} = 3011$ (m), 2956 (m), 2933 (m), 2856 (m), 2167 (w), 1606 (s), 1561 (m), 1522 (m), 1472 (m), 1462 (w), 1448 (w), 1361 (m), 1256 (s), 1106 (m), 1006 (w), 944 (w), 839 (s) cm^{-1}; Raman ($CHCl_3$): $\tilde{\nu} = 2925$ (w), 2400 (w), 2156 (m), 1605 (w), 1557 (m), 1370 (w), 1214 (m), 1144 (w), 970 (w), 762 (m), 665 (s), 364 (s), 259 (s) cm^{-1}; UV/Vis ($CHCl_3$): $\lambda = 287$ (40800), 427 (86800); MALDI-TOF-MS (THA, AHC): *m*/*z* (%): 1712.8 (43, $[M+Na]^+$), 1690.3 (100, $[M]^+$; calcd $^{12}C_{95}{}^{13}CH_{156}N_2O_8{}^{28}Si_7{}^{29}Si$: 1691.0), 1632.4 (53, $[M-C(CH_3)_3]^+$), 1558.0 (47, $[M-OSi(CH_3)_2C(CH_3)_3]^+$); $C_{96}H_{156}N_2O_8Si_8$ (1691.01): calcd C 68.19, H 9.30, N 1.66; found: C 68.01, H 9.14, N 1.61.

(*E*,*E*,*E*,*E*)-3,4,9,10,15,16,21,22,27,28-Decakis{[(*tert*-butyl)dimethylsilyloxy]methyl}-1,30-bis[4-(dimethylamino)phenyl]triaconta-3,9,15,21,27-pentaene-1,5,7,11,13,17,19,23,25,29-decayne (4e): Red solid (0.011 g, 4%); m.p. >200 °C (decoloration from red to deep red), 225–228 °C (decomp.); ^{1}H NMR (500 MHz, $CDCl_3$): $\delta = 0.088$ (s, 12H), 0.091 (s, 12H), 0.094 (s, 12H), 0.101 (s, 12H), 0.113 (s, 12H), 0.900 (s, 18H), 0.901 (s, 18H), 0.904 (s, 18H), 0.908 (s, 18H), 0.915 (s, 18H), 2.98 (s, 12H), 4.44 (s, 8H), 4.45 (s, 4H), 4.49 (s, 4H), 4.55 (s, 4H), 6.62 (d, $J = 9.0$ Hz, 4H), 7.30 (d, $J = 9.0$ Hz, 4H); ^{13}C NMR (125.8 MHz, $CDCl_3$): $\delta = -5.14$, -5.08, -5.07, 18.35, 18.41, 18.44, 25.88, 25.95, 40.12, 63.87, 63.89, 63.95, 64.32, 81.55, 83.01, 83.43, 84.46, 84.59, 85.57, 86.99, 87.44, 88.17, 105.91, 109.70, 111.75, 125.81, 131.62, 132.32, 132.79 (overlap, 2 signals), 134.77, 150.44; FT-IR ($CHCl_3$): $\tilde{\nu} = 3022$ (m), 2956 (m), 2933 (m), 2856 (m), 2400 (w), 2167 (w), 1606 (s), 1561 (m), 1522 (m), 1472 (m), 1462 (w), 1448 (w), 1361 (m), 1256 (s), 1106 (m), 1006 (w), 944 (w), 839 (s) cm^{-1}; Raman ($CHCl_3$): $\tilde{\nu} = 2925$ (w), 2400 (w), 2156 (m), 1605 (w), 1557 (m), 1367 (w), 1214 (m), 1142 (w), 961 (w), 762 (m), 665 (s), 364 (s), 259 (s) cm^{-1}; UV/Vis ($CHCl_3$): $\lambda = 288$ (44700), 428 (97900); MALDI-TOF-MS (THA, AHC): *m*/*z* (%): 2076.1 (31, $[M+Na]^+$), 2053.8 (100, $[M]^+$; calcd $^{12}C_{115}{}^{13}CH_{190}N_2O_{10}{}^{28}Si_9{}^{29}Si^+$: 2053.2), 1995.8 (15, $[M-C(CH_3)_3]^+$), 1921.5 (68, $[M-OSi(CH_3)_2C(CH_3)_3]^+$); $C_{116}H_{190}N_2O_{10}Si_{10}$ (2053.67): calcd C 67.84, H 9.32, N 1.36; found: C 67.55, H 9.44, N 1.25.

(*E*,*E*,*E*,*E*,*E*,*E*)-3,4,9,10,15,16,21,22,27,28,33,34-Dodecakis{[(*tert*-butyl)dimethylsilyloxy]methyl}-1,36-bis[4-(dimethylamino)phenyl]hexatriaconta-3,9,15,21,27,33-hexaene-1,5,7,11,13,17,19,23,25,29,31,35-dodecayne (4f): Red solid (0.008 mg, 2%); m.p. >200 °C (decoloration from red to deep red), 245–250 °C (decomp.); ^{1}H NMR (500 MHz, $CDCl_3$): $\delta = 0.086$ (s, 24H), 0.090 (s, 12H), 0.093 (s, 12H), 0.100 (s, 12H), 0.113 (s, 12H), 0.898 (s, 36H), 0.900 (s, 18H), 0.904 (s, 18H), 0.907 (s, 18H), 0.915 (s, 18H), 2.98 (s, 12H), 4.44 (s, 12H), 4.45 (s, 4H), 4.49 (s, 4H), 4.55 (s, 4H), 6.62 (d, $J = 9.0$ Hz, 4H), 7.30 (d, $J = 9.0$ Hz, 4H); ^{13}C NMR (125.8 MHz, $CDCl_3$): $\delta = -5.15$, -5.08, -5.06, 18.35, 18.41, 18.44, 25.87, 25.88, 25.95, 40.12, 63.86, 63.89, 63.95, 64.32, 81.53, 82.96, 83.22, 83.48, 84.46, 84.61, 85.57, 86.96, 87.31, 87.52, 88.19, 105.92, 109.69, 111.74, 125.80, 131.60, 132.25, 132.45, 132.79 (overlap, 2 signals), 134.78, 150.44; FT-IR ($CHCl_3$): $\tilde{\nu} = 3022$ (m), 2956 (m), 2933 (m), 2856 (m), 2370 (w), 2333 (w), 2167 (w), 1606 (s), 1561 (m), 1522 (m), 1472 (m), 1462 (w), 1361 (m), 1256 (s), 1106 (m), 1006 (w), 944 (w), 839 (s) cm^{-1}; Raman ($CHCl_3$): $\tilde{\nu} = 2925$ (w), 2400 (w), 2156 (m), 1605 (w), 1557 (m), 1364 (w), 1214 (m), 1137 (w), 961 (w), 763 (m), 665 (s), 364 (s), 259 (s) cm^{-1}; UV/Vis ($CHCl_3$): $\lambda = 286$ (49300), 431 (109400); MALDI-TOF-MS (THA, AHC): *m*/*z* (%): 2439.2 (73, $[M+Na]^+$), 2416.6 (100, $[M]^+$; calcd $^{12}C_{135}{}^{13}CH_{224}N_2O_{12}{}^{28}Si_{11}{}^{29}Si^+$: 2415.4), 2359.8 (19, $[M-C(CH_3)_3]^+$), 2285.3 (65, $[M-OSi(CH_3)_2C(CH_3)_3]^+$); $C_{136}H_{224}N_2O_{12}Si_{12}$ (2416.33): calcd C 67.60, H 9.34, N 1.16; found: C 67.46, H 9.08, N 1.23.

***α*,*ω*-[4-(Dimethylamino)phenyl]poly[(*E*)-3,4-bis{[(*tert*-butyl)dimethylsilyloxy]methyl}hex-3-ene-1,5-diyne] (4g)**: Red solid (0.029 g, 3%); m.p. >200 °C (decoloration from red to deep red), >240 °C (decomp.); DSC: 205 °C (decomp.); ^{1}H NMR (500 MHz, $CDCl_3$): $\delta = 0.09–0.11$ (overlap), 0.89–0.91 (overlap), 2.98 (br s), 4.44–4.45 (overlap), 4.49 (br s), 4.55 (br s), 6.62 (br d, $J = 9.0$ Hz), 7.30 (br d, $J = 9.0$ Hz); ^{13}C NMR (125.8 MHz, $CDCl_3$, $Cr(acac)_3$ added): $\delta = -5.27$ (overlap), 18.23 (overlap), 25.75 (overlap), 40.04, 63.73 (overlap), 63.83 (overlap), 64.20 (overlap), 81.42 (overlap), 82.81 (overlap), 83.11 (overlap), 84.34, 84.50, 85.45, 86.82, 87.03, 87.14–87.44 (overlap), 88.10, 96.11, 105.82, 109.56, 111.63, 125.54 (overlap), 125.66, 127.29–128.10 (overlap), 128.66, 131.47, 132.11, 132.28 (overlap), 132.68 (overlap), 134.67, 150.32; FT-IR ($CHCl_3$): $\tilde{\nu} = 2956$ (m), 2933 (m), 2856 (m), 2167 (w), 1606 (m), 1522 (m), 1472 (m), 1462 (m), 1361 (m), 1261 (m), 1006 (m), 939 (w), 839 (s) cm^{-1}; Raman ($CHCl_3$): $\tilde{\nu} = 3017$ (w), 2400 (w), 2156 (m), 1605 (w), 1556 (m), 1214 (m), 761 (m), 665 (s), 364 (s), 259 (s) cm^{-1}; UV/Vis ($CHCl_3$): $\lambda = 280$ (76200), 441 (180500); MALDI-TOF-MS (THA, AHC): *m*/*z* (%): 6065.2 (15, $[M+Na]^+$; calcd $^{12}C_{333}{}^{13}C_3H_{564}N_2O_{32}{}^{28}Si_{30}{}^{29}Si^{30}SiNa^+$ ($n = 16$): 6064.5), 5702.5 (25, $[M+Na]^+$; calcd $^{12}C_{313}{}^{13}C_3H_{530}N_2O_{30}{}^{28}Si_{28}{}^{29}Si^{30}SiNa^+$ ($n = 15$): 5702.3), 5339.6 (46, $[M+Na]^+$; calcd $^{12}C_{293}{}^{13}C_3H_{496}N_2O_{28}{}^{28}Si_{26}{}^{29}Si^{30}SiNa^+$ ($n = 14$): 5340.1), 4977.6 (71, $[M+Na]^+$; calcd $^{12}C_{273}{}^{13}C_3H_{462}N_2O_{26}{}^{28}Si_{24}{}^{29}Si^{30}SiNa^+$ ($n = 13$): 4977.9), 4615.4 (100, $[M+Na]^+$; calcd $^{12}C_{253}{}^{13}C_3H_{428}N_2O_{24}{}^{28}Si_{22}{}^{29}Si^{30}SiNa^+$ ($n = 12$): 4615.7), 4252.5 (97, $[M+Na]^+$; calcd $^{12}C_{234}{}^{13}C_2H_{394}N_2O_{22}{}^{28}Si_{20}{}^{29}Si^{30}SiNa^+$ ($n = 11$): 4252.5), 3889.1 (42, $[M+Na]^+$; calcd $^{12}C_{214}{}^{13}C_2H_{360}N_2O_{20}{}^{28}Si_{18}{}^{29}Si^{30}SiNa^+$ ($n = 10$): 3890.3); $C_{236}H_{394}N_2O_{22}Si_{22}$ ($n = 11$, 4229.56): calcd C 67.02, H 9.39, N 0.66; found: C 67.15, H 9.24, N 0.53; SEC [THF, 45 °C, refractive index (RI) detector]: $M_w = 13200$, $M_n = 6460$ ($M_w/M_n = 2.04$).

A–A oligomers 5b–f and polymer 5g: TMEDA (0.025 g, 0.03 mL, 0.22 mmol) and CuCl (0.006 g, 0.062 mmol) were added at 20 °C to a solution of **7** (0.149 g, 0.31 mmol) and **11** (0.028 g, 0.077 mmol) in dry CH_2Cl_2 (30 mL, containing 4 Å molecular sieves). After the solution was stirred in air for 2 h, an EDTA solution (pH 8, 100 mL) was added, and the mixture extracted with CH_2Cl_2 until the washings were colorless. The organic phase was washed with saturated aqueous NaCl solution (100 mL) and dried ($MgSO_4$). Concentration in vacuo, followed by purification using size-exclusion chromatography, and precipitation from MeOH gave the A–A oligomers **5b–f** and polymer **5g** as solids.

0947-6539/00/0623-4410 $ 17.50+.50/0 *Chem. Eur. J.* **2000**, *6*, No. 23

(*E*,*E*)-3,4,9,10-Tetrakis{[(*tert*-butyl)dimethylsilyloxy]methyl}-1,12-bis(4-nitrophenyl)dodeca-3,9-diene-1,5,7,11-tetrayne (5b): Yellow solid (0.093 g, 62%); m.p. 146–147°C; ^{1}H NMR (500 MHz, $CDCl_3$): $\delta = 0.12$ (s, 24H), 0.914 (s, 18H), 0.918 (s, 18H), 4.53 (s, 4H), 4.54 (s, 4H), 7.56 (d, $J = 8.8$ Hz, 4H), 8.20 (d, $J = 8.8$ Hz, 4H); ^{13}C NMR (125.8 MHz, $CDCl_3$): $\delta = -5.15$, 18.36, 18.39, 25.85, 25.87, 63.88, 63.95, 82.55, 86.08, 91.51, 100.67, 123.75, 129.63, 130.29, 132.08, 132.73, 147.27; FT-IR ($CHCl_3$): $\tilde{\nu} = 2956$ (m), 2932 (m), 2856 (m), 2189 (w), 1595 (m), 1522 (m), 1472 (m), 1460 (m), 1345 (s), 1261 (m), 1106 (m), 1006 (w), 856 (m), 839 (s) cm^{-1}; Raman ($CHCl_3$): $\tilde{\nu} =$ 2925 (w), 2399 (w), 2170 (m), 1591 (m), 1565 (m), 1342 (m), 1214 (m), 1163 (w), 1106 (w), 1011 (w), 972 (w), 876 (w), 761 (m), 665 (s), 364 (s), 259 (s) cm^{-1}; UV/Vis ($CHCl_3$): $\lambda = 303$ (27500), 395 (56500); FAB-MS: *m*/*z* (%): 968.5 (20, $[M]^+$; calcd $^{12}C_{52}H_{76}N_2O_8{}^{28}Si_4$: 968.5), 911.4 (28, $[M - C(CH_3)_3]^+$), 837.4 (37, $[M - OSi(CH_3)_2C(CH_3)_3]^+$), 72.9 (100, $[Si(CH_3)_3]^+$); $C_{52}H_{76}N_2O_8Si_4$ (969.54): calcd C 64.42, H 7.90, N 2.89; found: C 64.24, H 7.72, N 2.89.

(*E*,*E*,*E*)-3,4,9,10,15,16-Hexakis{[(*tert*-butyl)dimethylsilyloxy]methyl}-1,18-bis(4-nitrophenyl)octadeca-3,9,15-triene-1,5,7,11,13,17-hexayne (5c): Yellow solid (0.041 g, 20%); m.p. 169–170°C; ^{1}H NMR (500 MHz, $CDCl_3$): $\delta = 0.103$ (s, 12H), 0.107 (s, 12H), 0.110 (s, 12H), 0.910–0.909 (overlap, 54H), 4.46 (s, 4H), 4.52 (s, 4H), 4.53 (s, 4H), 7.55 (d, $J = 8.9$ Hz, 4H), 8.20 (d, $J = 8.9$ Hz, 4H); ^{13}C NMR (125.8 MHz, $CDCl_3$): $\delta = -5.15$, -5.11, 18.35, 18.38, 25.85, 25.87, 63.88, 63.95, 82.63, 83.17, 86.12, 87.30, 91.56, 100.68, 123.75, 129.65, 130.31, 132.08, 132.43, 132.74, 147.32; FT-IR ($CHCl_3$): $\tilde{\nu} = 3011$ (m), 2956 (m), 2933 (m), 2856 (m), 2341 (w), 2181 (w), 1594 (m), 1522 (m), 1472 (m), 1344 (s), 1256 (m), 1106 (m), 1006 (w), 939 (w), 839 (s) cm^{-1}; Raman ($CHCl_3$): $\tilde{\nu} = 2925$ (w), 2399 (w), 2166 (m), 1563 (m), 1343 (m), 1214 (m), 1153 (w), 1106 (w), 970 (w), 876 (w), 762 (m), 665 (s), 364 (s), 259 (s) cm^{-1}; UV/Vis ($CHCl_3$): $\lambda = 315$ (32100), 407 (75700); MALDI-TOF-MS (THA, AHC): *m*/*z* (%): 1353.7 (12, $[M+Na]^+$), 1330.5 (26, $[M]^+$; calcd $^{12}C_{72}H_{110}N_2O_{10}{}^{28}Si_6{}^+$: 1330.7), 1274.4 (100, $[M - C(CH_3)_3]^+$); $C_{72}H_{110}N_2O_{10}Si_6$ (1332.20): calcd C 64.92, H 8.32, N 2.10; found: C 64.97, H 8.19, N 2.18.

(*E*,*E*,*E*,*E*)-3,4,9,10,15,16,21,22-Octakis{[(*tert*-butyl)dimethylsilyloxy]methyl}-1,24-bis(4-nitrophenyl)tetracosa-3,9,15,21-tetraene-1,5,7,11,13,17,19,23-octayne (5d): Deep yellow solid (0.019 g, 7%); m.p. 222–223°C; ^{1}H NMR (500 MHz, $CDCl_3$): $\delta = 0.095$ (s, 12H), 0.097 (s, 12H), 0.105 (s, 12H), 0.108 (s, 12H), 0.905 (s, 18H), 0.908–0.914 (overlap, 54H), 4.45 (s, 8H), 4.51 (s, 4H), 4.53 (s, 4H), 7.55 (d, $J = 9.0$ Hz, 4H), 8.20 (d, $J = 9.0$ Hz, 4H); ^{13}C NMR (125.8 MHz, $CDCl_3$): $\delta = -5.15$, -5.11, 18.36, 18.38, 25.86, 25.88, 63.90, 63.97, 82.70, 83.21, 83.26, 86.15, 87.31, 87.35, 91.60, 100.67, 123.75, 129.68, 130.34, 132.08, 132.445, 132.454, 132.75, 147.36; FT-IR ($CHCl_3$): $\tilde{\nu} =$ 2951 (m), 2929 (m), 2852 (m), 2192 (w), 1596 (m), 1519 (m), 1473 (m), 1464 (m), 1343 (s), 1260 (m), 1106 (m), 1007 (w), 836 (s) cm^{-1}; Raman ($CHCl_3$): $\tilde{\nu} = 2925$ (w), 2399 (w), 2164 (m), 1560 (m), 1343 (w), 1214 (m), 1106 (w), 962 (w), 876 (w), 762 (m), 665 (s), 364 (s), 259 (s) cm^{-1}; UV/Vis ($CHCl_3$): $\lambda = 260$ (49600), 304 (43100), 417 (95300); MALDI-TOF-MS (THA, AHC): *m*/*z* (%): 1718.4 (49, $[M+Na]^+$), 1694.7 (50, $[M]^+$; calcd $^{12}C_{91}{}^{13}CH_{144}N_2O_{12}{}^{28}Si_7{}^{29}Si^+$: 1694.9), 1637.6 (100, $[M - C(CH_3)_3]^+$); $C_{92}H_{144}N_2O_{12}Si_8$ (1694.86): calcd C 65.20, H 8.56, N 1.65; found: C 65.41, H 8.40, N 1.78.

(*E*,*E*,*E*,*E*)-3,4,9,10,15,16,21,22,27,28-Decakis{[(*tert*-butyl)dimethylsilyloxy]methyl}-1,30-bis(4-nitrophenyl)triaconta-3,9,15,21,27-pentaene-1,5,7,11,13,17,19,23,25,29-decayne (5e): Deep yellow solid (0.011 g, 3%); m.p. 227–229°C; ^{1}H NMR (500 MHz, $CDCl_3$): $\delta = 0.089$ (s, 12H), 0.093 (s, 12H), 0.095 (s, 12H), 0.104 (s, 12H), 0.107 (s, 12H), 0.900 (s, 18H), 0.903 (s, 18H), 0.907 (overlap, 54H), 4.44 (s, 4H), 4.45 (s, 8H), 4.51 (s, 4H), 4.53 (s, 4H), 7.55 (d, $J = 9.0$ Hz, 4H), 8.20 (d, $J = 9.0$ Hz, 4H); ^{13}C NMR (125.8 MHz, $CDCl_3$): $\delta = -5.15$, -5.10, 18.36, 18.39, 25.87, 25.88, 63.90, 63.97, 82.71, 83.20, 83.26, 83.29, 86.16, 87.31, 87.37 (overlap, 2 signals), 91.61, 100.67, 123.75, 129.68, 130.34, 132.08, 132.44, 132.45, 132.46, 132.75, 147.36; FT-IR ($CHCl_3$): $\tilde{\nu} = 2956$ (m), 2933 (m), 2856 (m), 2189 (w), 1594 (m), 1522 (m), 1472 (m), 1463 (m), 1344 (s), 1256 (m), 1106 (m), 1006 (w), 839 (s) cm^{-1}; Raman ($CHCl_3$): $\tilde{\nu} = 2925$ (w), 2399 (w), 2163 (m), 1559 (m), 1497 (w), 1342 (w), 1214 (m), 876 (w), 762 (m), 665 (s), 364 (s), 259 (s) cm^{-1}; UV/Vis ($CHCl_3$): $\lambda = 423$ (112400); MALDI-TOF-MS (THA, AHC): *m*/*z* (%): 2080.7 (79, $[M+Na]^+$), 2057.2 (55, $[M]^+$; calcd $^{12}C_{111}{}^{13}CH_{178}N_2O_{14}{}^{28}Si_9{}^{29}Si^+$: 2057.1), 2000.3 (100, $[M - C(CH_3)_3]^+$); $C_{112}H_{178}N_2O_{14}Si_{10}$ (2057.53): calcd C 65.38, H 8.72, N 1.36; found: C 65.27, H 8.68, N 1.44.

(*E*,*E*,*E*,*E*,*E*)-3,4,9,10,15,16,21,22,27,28,33,34-Dodecakis{[(*tert*-butyl)dimethylsilyloxy]methyl}-1,36-bis(4-nitrophenyl)hexatriaconta-3,9,15,21,27,33-hexaene-1,5,7,11,13,17,19,23,25,29,31,35-dodecayne (5f): Deep yellow solid (0.009 g, 2%); m.p. 240–242°C; ^{1}H NMR (500 MHz, $CDCl_3$): $\delta =$ 0.087 (s, 24H), 0.092 (s, 12H), 0.094 (s, 12H), 0.104 (s, 12H), 0.107 (s, 12H), 0.898 (s, 18H), 0.902 (s, 18H), 0.905–0.907 (overlap, 72H), 4.44 (s, 8H), 4.45 (s, 8H), 4.51 (s, 4H), 4.53 (s, 4H), 7.55 (d, $J = 9.0$ Hz, 4H), 8.20 (d, $J =$ 9.0 Hz, 4H); ^{13}C NMR (125.8 MHz, $CDCl_3$): $\delta = -5.15$, -5.11, 18.36, 18.39, 25.88, 63.89, 63.98, 82.71, 83.20, 83.26, 83.30 (overlap, 2 signals), 86.16, 87.30, 87.35, 87.38 (overlap, 2 signals), 91.61, 100.67, 123.75, 129.68, 130.34, 132.08, 132.43 (overlap, 2 signals), 132.45, 132.47, 132.75, 147.36; FT-IR ($CHCl_3$): $\tilde{\nu} = 3022$ (m), 2957 (m), 2933 (m), 2856 (m), 2189 (w), 1594 (m), 1522 (m), 1472 (m), 1463 (m), 1344 (m), 1261 (m), 1106 (m), 1006 (w), 939 (w), 828 (s) cm^{-1}; Raman ($CHCl_3$): $\tilde{\nu} = 2925$ (w), 2399 (w), 2162 (m), 1558 (m), 1496 (w), 1343 (w), 1214 (m), 876 (w), 761 (m), 665 (s), 364 (s), 259 (s) cm^{-1}; UV/Vis ($CHCl_3$): $\lambda = 425$ (132300); MALDI-TOF-MS (THA, AHC): *m*/*z* (%): 2442.8 (100, $[M+Na]^+$), 2419.3 (46, $[M]^+$; calcd $^{12}C_{131}{}^{13}CH_{212}N_2O_{16}{}^{28}Si_{11}{}^{29}Si^+$: 2419.3), 2362.8 (79, $[M - C(CH_3)_3]^+$); $C_{132}H_{212}N_2O_{16}Si_{12}$ (2420.19): calcd C 65.51, H 8.83, N 1.16; found: C 65.41, H 8.80, N 1.24.

***α*,*ω*-Bis(4-nitrophenyl)poly[(*E*)-3,4-bis{[(*tert*-butyl)dimethylsilyloxy]methyl}hex-3-ene-1,5-diyne] (5g)**: Deep yellow/orange solid (0.028 g, 4%); m.p. >20°C (decoloration from yellow to brown), >240°C (decomp.); DSC: 193°C (decomp.); ^{1}H NMR (500 MHz, $CDCl_3$): $\delta = 0.08$–0.12 (overlap), 0.90–0.91 (overlap), 4.44–4.45 (overlap), 4.51 (br s), 4.53 (br s), 7.55 (br d, $J = 8.9$ Hz), 8.20 (br d, $J = 8.9$ Hz); ^{13}C NMR (125.8 MHz, $CDCl_3$, $Cr(acac)_3$ added): $\delta = -5.46$ (overlap), 18.05 (overlap), 25.57 (overlap), 63.55 (overlap), 82.92 (overlap), 85.84, 87.06 (overlap), 91.25, 100.37, 123.49, 129.34 (overlap), 130.00 (overlap), 131.81 (overlap), 132.08 (overlap), 132.40 (overlap), 146.98; FT-IR ($CHCl_3$): $\tilde{\nu} =$ 3016 (m), 2953 (m), 2930 (m), 2885 (w), 2856 (m), 2399 (w), 1595 (m), 1520 (m), 1472 (m), 1463 (m), 1361 (w), 1343 (m), 1267 (m), 1106 (m), 1006 (w), 838 (s) cm^{-1}; Raman ($CHCl_3$): $\tilde{\nu} = 3017$ (w), 2400 (w), 2158 (m), 1557 (m), 1214 (m), 762 (m), 665 (s), 364 (s), 259 (s) cm^{-1}; UV/Vis ($CHCl_3$): $\lambda = 286$ (72300), 437 (191000); MALDI-TOF-MS (IAA): *m*/*z* (%): 6066.9 (7, $[M+Na]^+$; calcd $^{12}C_{329}{}^{13}C_3H_{552}N_2O_{36}{}^{28}Si_{30}{}^{29}Si^{30}SiNa^+$ ($n = 16$): 6068.4), 5708.5 (13, $[M+Na]^+$; calcd $^{12}C_{309}{}^{13}C_3H_{518}N_2O_{34}{}^{28}Si_{28}{}^{29}Si^{30}SiNa^+$ ($n = 15$): 5706.2), 5345.3 (18, $[M+Na]^+$; calcd $^{12}C_{289}{}^{13}C_3H_{484}N_2O_{32}{}^{28}Si_{26}{}^{29}Si^{30}SiNa^+$ ($n = 14$): 5344.0), 4983.8 (31, $[M+Na]^+$; calcd $^{12}C_{269}{}^{13}C_3H_{450}N_2O_{30}{}^{28}Si_{24}{}^{29}Si^{30}SiNa^+$ ($n = 13$): 4981.8), 4620.6 (46, $[M+Na]^+$; calcd $^{12}C_{249}{}^{13}C_3H_{416}N_2O_{28}{}^{28}Si_{22}{}^{29}Si^{30}SiNa^+$ ($n = 12$): 4619.6), 4259.2 (74, $[M+Na]^+$; calcd $^{12}C_{230}{}^{13}C_2H_{382}N_2O_{26}{}^{28}Si_{20}{}^{29}Si^{30}SiNa^+$ ($n = 11$): 4256.3), 3896.6 (100, $[M+Na]^+$; calcd $^{12}C_{210}{}^{13}C_2H_{348}N_2O_{24}{}^{28}Si_{18}{}^{29}Si^{30}SiNa^+$ ($n = 10$): 3894.1), 3533.7 (85, $[M+Na]^+$; calcd $^{12}C_{190}{}^{13}C_2H_{314}N_2O_{22}{}^{28}Si_{17}{}^{29}SiNa^+$ ($n = 9$): 3529.9); $C_{212}H_{348}N_2O_{24}Si_{20}$ ($n = 10$, 3870.85): C 65.78, H 9.06, N 0.72; found: C 65.75, H 9.25, N 0.93; SEC (THF, 45°C, RI-detector): $M_w = 7230$, $M_n =$ 4390 ($M_w/M_n = 1.65$).

D–D, D–A, and A–A dimers 4b, 12b, and 5b: TMEDA (0.049 g, 0.06 mL, 0.42 mmol) and CuCl (0.012 g, 0.12 mmol) were added at 20°C to a solution of **6** (0.11 g, 0.23 mmol) and **7** (0.11 g, 0.23 mmol) in dry toluene (10 mL, containing 4 Å molecular sieves). After the reaction mixuture was stirred in air for 2 h, an EDTA solution (pH 8, 100 mL) was added and the mixture was extracted with CH_2Cl_2 until the washings were colorless. The organic phase was washed with saturated aqueous NaCl solution (100 mL) and dried ($MgSO_4$). Concentration in vacuo, purification by CC (SiO_2-*H*, eluent: *n*-hexane/ethyl acetate 10:1), and preparative thin-layer chromatography (SiO_2–60, eluent: *n*-hexane/ethyl acetate 10:1+1% NEt_3) afforded the pure oligomers **4b** (0.028 g, 12%), **12b** (see below), and **5b** (0.053 g, 24%).

(*E*,*E*)-3,4,9,10-Tetrakis{[(*tert*-butyl)dimethylsilyloxy]methyl}-12-[4-(dimethylamino)phenyl]-1-(*p*-nitrophenyl)dodeca-3,9-diene-1,5,7,11-tetrayne (12b): Deep red solid (0.069 g, 29%); m.p. 188–189°C; ^{1}H NMR (500 MHz, $CDCl_3$): $\delta = 0.112$ (s, 6H), 0.115 (s, 12H), 0.123 (s, 6H), 0.91 (s, 9H), 0.918 (s, 18H), 0.923 (s, 9H), 2.98 (s, 6H), 4.51 (s, 2H), 4.53 (s, 4H), 4.56 (s, 2H), 6.62 (d, $J = 9.0$ Hz, 2H), 7.31 (d, $J = 9.0$ Hz, 2H), 7.55 (d, $J =$ 8.9 Hz, 2H), 8.19 (d, $J = 8.9$ Hz, 2H); ^{13}C NMR (125.8 MHz, $CDCl_3$): $\delta =$ -5.09, -5.08, -5.07, 18.36, 18.40, 18.44, 25.86, 25.89, 25.95, 40.11, 63.90, 63.95, 63.96, 64.33, 81.43, 84.00, 84.37, 85.53, 86.95, 91.84, 100.28, 105.94, 109.65, 111.74, 123.73, 125.77, 129.83, 130.69, 131.92, 132.04, 132.79, 134.80, 147.20, 150.45; FT-IR ($CHCl_3$): $\tilde{\nu} = 3022$ (w), 2956 (m), 2933 (m), 2856 (m), 2167 (m), 1606 (m), 1561 (m), 1522 (m), 1472 (m), 1460 (m), 1344 (s), 1256 (m), 1161 (m), 1106 (m), 1033 (w), 1006 (w), 944 (w), 839 (s); Raman ($CHCl_3$): $\tilde{\nu} = 2925$ (w), 2399 (w), 2163 (m), 1562 (m), 1342 (w), 1214 (m), 1159 (w), 972 (w), 761 (m), 665 (s), 364 (s), 259 (s); UV/Vis ($CHCl_3$): $\lambda =$

291 (28500), 399 (53300), 442 (39600, sh); FAB-MS: *m/z* (%): 966.5 (45, $[M]^+$; calcd $^{12}C_{54}H_{82}N_2O_6{}^{28}Si_4{}^+$: 966.5), 909.4 (5, $[M-C(CH_3)_3]^+$), 835.4 (11, $[M-OSi(CH_3)_2C(CH_3)_3]^+$), 72.9 (100, $[Si(CH_3)_3]^+$); $C_{54}H_{82}N_2O_6Si_4$ (967.61): C 67.03, H 8.54, N 2.90; found: C 66.83, H 8.59, N 2.78.

(*E*)-3,4-Bis{[(*tert*-butyl)dimethylsilyloxy]methyl}-1-(4-nitrophenyl)hex-3-ene-1,5-diyne (7): K_2CO_3 (0.23 g, 1.70 mmol) was added to a solution of **10** (0.32 g, 0.57 mmol) in THF/MeOH (30 mL, 1:1). The solution was stirred for 2 h at 20 °C and extracted with CH_2Cl_2 (200 mL). The organic phase was washed with saturated aqueous NaCl solution (100 mL), and subsequently dried ($MgSO_4$). Removal of the solvent in vacuo gave **7** (0.27 g, 97%) as a pale yellow solid; m.p. 82–83 °C; ^{1}H NMR (300 MHz, $CDCl_3$): $\delta = 0.10$ (s, 12H), 0.90 (s, 18H), 3.60 (s, 1H), 4.51 (s, 2H), 4.53 (s, 2H), 7.55 (d, $J =$ 9.0 Hz, 2H), 8.19 (d, $J = 9.0$ Hz, 2H); ^{13}C NMR (75.5 MHz, $CDCl_3$): $\delta =$ −5.31, −5.25, 18.24, 18.31, 25.73, 25.77, 63.67, 64.01, 80.32, 89.77, 91.29, 98.66, 123.80, 129.92, 130.32, 130.89, 132.15, 147.29; FT-IR ($CHCl_3$): $\tilde{\nu} =$ 3300 (m), 3027 (m), 3009 (m), 2958 (m), 2931 (m), 2856 (w), 2439 (w), 2396 (w), 2303 (w), 2192 (w), 1598 (s), 1522 (s), 1472 (w), 1460 (w), 1346 (s), 1265 (m), 1139 (w), 1106 (m), 1006 (w), 932 (w), 894 (w), 855 (m), 838 (s) cm^{-1}; Raman ($CHCl_3$): $\tilde{\nu} = 2925$ (w), 2399 (w), 2197 (w), 2133 (w), 1961 (w), 1572 (w), 1496 (w), 1341 (w), 1214 (m), 1106 (w), 876 (w), 761 (m), 665 (s), 364 (s), 259 (s) cm^{-1}; UV/Vis ($CHCl_3$): $\lambda = 270$ (8000), 343 (13500); EI-MS: *m/z* (%): 428.1 (14, $[M-C(CH_3)_3]^+$; calcd $^{12}C_{22}H_{30}NO_4{}^{28}Si_2{}^+$: 428.2), 84.0 (100), 73.0 (77, $[Si(CH_3)_3]^+$); $C_{26}H_{39}NO_4Si_2$ (485.78): calcd C 64.29, H 8.09, N 2.88; found: C 64.00, H 7.99, N 2.84.

(*E*)-3,4-Bis{[(*tert*-butyl)dimethylsilyloxy]methyl}-1-(4-nitrophenyl)-6-(trimethylsilyl)hex-3-ene-1,5-diyne (10): A mixture of **8** (0.27 g, 0.61 mmol), 4-iodonitrobenzene (0.18 g, 0.73 mmol), $[PdCl_2(PPh_3)_2]$ (0.021 g, 0.030 mmol), and CuI (0.007 g, 0.037 mmol, 0.06 equiv) in degassed NEt_3 (5 mL) and CH_2Cl_2 (20 mL) was stirred at 20 °C for 24 h. The solvent and NEt_3 were removed in vacuo, and the resulting residue was passed through a plug (SiO_2–60, eluent: CH_2Cl_2). CC (SiO_2-*H*, eluent: *n*-hexane/ethyl acetate 15:1) of the crude reaction mixture and removal of remaining 4-iodonitrobenzene by crystallization from *n*-hexane gave pure **10** (0.30 g, 95%) as a pale yellow solid; m.p. 74–75 °C; ^{1}H NMR (300 MHz, $CDCl_3$): $\delta = 0.08$ (s, 12H), 0.19 (s, 9H), 0.89 (s, 18H), 4.47 (s, 2H), 4.52 (s, 2H), 7.53 (d, $J = 8.6$ Hz, 2H), 8.17 (d, $J = 8.6$ Hz, 2H); ^{13}C NMR (75.5 MHz, $CDCl_3$): $\delta =$ −5.30, −5.26, −0.38, 18.24, 18.29, 25.77, 63.86, 91.72, 98.79, 101.49, 108.35, 123.76, 129.90, 130.10, 131.44, 132.12, 147.20; FT-IR ($CHCl_3$): $\tilde{\nu} =$ 2956 (m), 2933 (m), 2856 (m), 2200 (w), 2133 (w), 1594 (s), 1522 (s), 1472 (w), 1460 (w), 1344 (s), 1256 (m), 1139 (w), 1106 (m), 1006 (w), 933 (s), 844 (s) cm^{-1}; Raman ($CHCl_3$): $\tilde{\nu} = 2925$ (w), 2399 (w), 2197 (w), 2133 (w), 1961 (w), 1572 (w), 1496 (w), 1341 (w), 1214 (m), 1106 (w), 876 (w), 761 (m), 665 (s), 364 (s), 259 (s) cm^{-1}; UV/Vis ($CHCl_3$): $\lambda = 283$ (15400), 354 (23800); EI-MS: *m/z* (%): 542.3 (0.02, $[M-CH_3]^+$; calcd $^{12}C_{28}H_{43}NO_4{}^{28}Si_3{}^+$: 542.3), 500.2 (10, $[M-C(CH_3)_3]^+$), 73.0 (100, $[Si(CH_3)_3]^+$); $C_{29}H_{47}NO_4Si_3$ (557.96): calcd C 62.43, H 8.49, N 2.51; found: C 62.14, H 8.27, N 2.43.

Acknowledgement

This work was supported by a grant ("TEMA") from the ETH Research Council. We would like to thank Prof. Rik R. Tykwinski (Univ. of Alberta) for the DSC measurements, Ms. Patrizia Fabrizoli for assistance with the Raman spectroscopy, and M. Colussi, Institut für Polymere, ETHZ, for the molecular weight determinations of the polymers.

[1] *Electronic Materials*: *The Oligomer Approach* (Eds.: K. Müllen, G. Wegner), Wiley-VCH, Weinheim, **1997**.
[2] J. Roncali, *Chem. Rev.* **1997**, *97*, 173–205.
[3] J. M. Tour, *Chem. Rev.* **1996**, *96*, 537–553.
[4] R. E. Martin, F. Diederich, *Angew. Chem.* **1999**, *111*, 1440–1469; *Angew. Chem. Int. Ed.* **1999**, *38*, 1350–1377.
[5] K. Müllen, *Pure Appl. Chem.* **1993**, *65*, 89–96.
[6] U. Scherf, K. Müllen, *Synthesis* **1992**, 23–38.
[7] R. E. Martin, U. Gubler, C. Boudon, V. Gramlich, C. Bosshard, J.-P. Gisselbrecht, P. Günter, M. Gross, F. Diederich, *Chem. Eur. J.* **1997**, *3*, 1505–1512.
[8] H. Meier, U. Stalmach, H. Kolshorn, *Acta Polym.* **1997**, *48*, 379–384.
[9] a) G. Zerbi, E. Galbiati, M. C. Gallazi, C. Castiglioni, M. Del Zoppo, R. Schenk, K. Müllen, *J. Chem. Phys.* **1996**, *105*, 2509–2516; b) J. Grimme, M. Kreyenschmidt, F. Uckert, K. Müllen, U. Scherf, *Adv. Mater.* **1995**, *7*, 292–295; c) J. Guay, P. Kasai, A. Diaz, R. L. Wu, J. M. Tour, L. H. Dao, *Chem. Mater.* **1992**, *4*, 1097–1105; d) S. A. Jenekhe, *Macromolecules* **1990**, *23*, 2848–2854; e) J. L. Brédas, R. Silbey, D. S. Boudreaux, R. R. Chance, *J. Am. Chem. Soc.* **1983**, *105*, 6555–6559.
[10] a) G. Klaerner, R. D. Miller, *Macromolecules* **1998**, *31*, 2007–2009; b) G. Klaerner, M. H. Davey, W. D. Chen, J. C. Scott, R. D. Miller, *Adv. Mater.* **1998**, *10*, 993–997; c) W. Li, T. Maddux, L. Yu, *Macromolecules* **1996**, *29*, 7329–7334.
[11] D. L. Pearson, J. M. Tour, *J. Org. Chem.* **1997**, *62*, 1376–1387.
[12] D. L. Pearson, J. S. Schumm, J. M. Tour, *Macromolecules* **1994**, *27*, 2348–2350.
[13] T. Kauffmann, H. Lexy, *Chem. Ber.* **1981**, *114*, 3674–3683.
[14] H.-P. Weitzel, A. Bohnen, K. Müllen, *Makromol. Chem.* **1990**, *191*, 2815–2835.
[15] R. E. Martin, T. Mäder, F. Diederich, *Angew. Chem.* **1999**, *111*, 834–838; *Angew. Chem. Int. Ed.* **1999**, *38*, 817–821.
[16] R. E. Martin, U. Gubler, J. Cornil, M. Balakina, C. Boudon, C. Bosshard, J.-P. Gisselbrecht, F. Diederich, P. Günter, M. Gross, J.-L. Brédas, *Chem. Eur. J.* **2000**, *6*, 3622–3635.
[17] R. R. Tykwinski, M. Schreiber, R. Pérez Carlón, F. Diederich, V. Gramlich, *Helv. Chim. Acta* **1996**, *79*, 2249–2281.
[18] M. Schreiber, PhD thesis, ETH, Zürich, No. 11904, **1996**.
[19] K. Sonogashira in *Metal-catalyzed Cross-coupling Reactions* (Eds.: F. Diederich, P. J. Stang), Wiley-VCH, New York, **1998**, pp. 203–227.
[20] R. E. Martin, J. Bartek, F. Diederich, R. R. Tykwinski, E. C. Meister, A. Hilger, H. P. Lüthi, *J. Chem. Soc. Perkin Trans. 2* **1998**, 233–241.
[21] M. Schreiber, J. Anthony, F. Diederich, M. E. Spahr, R. Nesper, M. Hubrich, F. Bommeli, L. Degiorgi, P. Wachter, P. Kaatz, C. Bosshard, P. Günter, M. Colussi, U. W. Suter, C. Boudon, J.-P. Gisselbrecht, M. Gross, *Adv. Mater.* **1994**, *6*, 786–790.
[22] J. Anthony, PhD thesis, University of California, Los Angeles, **1993**.
[23] A. S. Hay, *J. Org. Chem.* **1962**, *27*, 3320–3321.
[24] K. Martin, J. Spickermann, H. J. Räder, K. Müllen, *Rapid Commun. Mass Spectrom.* **1996**, *10*, 1471–1474.
[25] F. Ammar, J. M. Savéant, *J. Electroanal. Chem. Interfacial Electrochem.* **1973**, *47*, 215–221.
[26] A. Hilger, J.-P. Gisselbrecht, R. R. Tykwinski, C. Boudon, M. Schreiber, R. E. Martin, H. P. Lüthi, M. Gross, F. Diederich, *J. Am. Chem. Soc.* **1997**, *119*, 2069–2078.
[27] a) A. M. Boldi, J. Anthony, C. B. Knobler, F. Diederich, *Angew. Chem.* **1992**, *104*, 1270–1273; *Angew. Chem. Int. Ed.* **1992**, *31*, 1240–1242; b) J. Anthony, C. Boudon, F. Diederich, J.-P. Gisselbrecht, V. Gramlich, M. Gross, M. Hobi, P. Seiler, *Angew. Chem.* **1994**, *106*, 794–798; *Angew. Chem. Int. Ed.* **1994**, *33*, 763–766.
[28] P. Bäuerle, *Adv. Mater.* **1992**, *4*, 102–107.
[29] E. H. Elandaloussi, P. Frére, P. Richomme, J. Orduna, J. Garin, J. Roncali, *J. Am. Chem. Soc.* **1997**, *119*, 10774–10784.
[30] R. Schenk, H. Gregorius, K. Meerholz, J. Heinze, K. Müllen, *J. Am. Chem. Soc.* **1991**, *113*, 2634–2647.
[31] J. Wytko, V. Berl, M. McLaughlin, R. R. Tykwinski, M. Schreiber, F. Diederich, C. Boudon, J.-P. Gisselbrecht, M. Gross, *Helv. Chim. Acta* **1998**, *81*, 1964–1977.
[32] C. Bosshard, R. Spreiter, P. Günter, R. R. Tykwinski, M. Schreiber, F. Diederich, *Adv. Mater.* **1996**, *8*, 231–234.
[33] J. Zyss, *Molecular Nonlinear Optics*: *Materials*, *Physics and Devices*, Academic Press, Boston, **1993**.
[34] Note that the γ value for **1a** with 9.2×10^{-36} esu differs from the previously published value of 22×10^{-36} esu, see ref. [7], owing to a change in the reference value for fused silica from $\chi^{(3)}_{fs} = 3.9 \times 10^{-22}$ m^2 V^{-2} to $\chi^{(3)}_{fs} = 1.6 \cdot 10^{-22}$ m^2 V^{-2}; U. Gubler, C. Bosshard, *Phys. Rev. B* **2000**, *61*, 10702–10710.
[35] U. Gubler, C. Bosshard, P. Günter, M. Y. Balakina, J. Cornil, J. L. Brédas, R. E. Martin, F. Diederich, *Opt. Lett.* **1999**, *24*, 1599–1601.
[36] A. F. Garito, J. R. Heflin, K. Y. Wong, O. Zamani-Khamiri in *Organic Materials for Non-linear Optics* (Eds.: R. A. Hann, D. Bloor), Royal Society of Chemistry, Oxford, **1989**, pp. 16–27.
[37] C. W. Dirk, L.-T. Cheng, M. G. Kuzyk, *Int. J. Quant. Chem.* **1992**, *43*, 27–36.

Received: July 18, 2000 [F2609]

  0947-6539/00/0623-4412 $ 17.50+.50/0